IEEE Access
Multidisciplinary | Rapid Review | Open Access Journal

Received January 18, 2020, accepted February 20, 2020, date of publication March 3, 2020, date of current version April 7, 2020.

Digital Object Identifier 10.1109/ACCESS.2020.2978161

A Group Analysis of Oscillatory Phase and Phase Synchronization in Cortical Networks

DAMING WANG[1], YAORU SUN[1], HAIBO SHI[2], AND FANG WANG[3]
[1]Laboratory of Cognition and Intelligent Computation, Department of Computer Science and Technology, Tongji University, Shanghai 201804, China
[2]School of Statistics and Management, Shanghai University of Finance and Economics, Shanghai 200433, China
[3]Department of Computer Science, Brunel University, Uxbridge UB8 3PH, U.K.

Corresponding author: Yaoru Sun (yaoru@tongji.edu.cn)

This work was supported in part by the National Key Research and Development Program of China under Grant 2016YFC1306805, in part by the National Natural Science Foundation of China under Grant 91748122, and in part by the Shanghai Science and Technology Committee under Grant 17JC1400603.

ABSTRACT Neuronal oscillatory phase and phase synchronization are two main aspects of neuronal oscillation. Neurophysiological and computational studies have demonstrated that oscillatory phase for individual neurons has quantifiable relationships with neuronal excitation and input stimulus. In order to investigate the issue for neuronal groups, we constructed orientation columns by means of a spiking neural network and introduced six network activity states, pre-stimulus and stimulus periods for comparison. We proposed a new method of spike-LFP (Local Field Potential) phase based on vector addition of point spike-LFP phases to represent oscillatory phase. We also proposed a PPCG (Pairwise Phase Consistency for Group) method to quantify phase synchronization for neuronal groups. As illustrated in the simulation, the characteristics of oscillatory phase and phase synchronization for neuronal groups were consistent with the ones for individual neurons. Preferred orientations and stronger external inputs tended to result in smaller and more concentrated oscillatory phases. No matter individual neurons or neuronal groups, the oscillatory phase decreased monotonically as a function of neuronal excitation and input strength. More importantly, neuronal groups had a competitive advantage over individual neurons, because they can achieve reliable relationship quantification of oscillatory phase for all network activity states, even in weak oscillatory or non-oscillatory states.

INDEX TERMS Neuronal oscillation, phase synchronization, spike-LFP phase, pairwise phase consistency for group PPCG, neuronal coherence, neuronal assembly, spiking neural network.

I. INTRODUCTION

Neuronal oscillation and synchronization, with various frequency bands, are ubiquitous phenomenon in several cortical and subcortical areas, ranging from visual cortex [1]–[3], motor cortex [4], prefrontal cortex [5]–[7], hippocampus [7]–[9] and thalamus [1] to somatosensory cortex [10], olfactory bulb [11] and amygdala [12]. They have been observed in a wide range of species, including insects [13], rodents [5], [11], [14], cats [15], non-human primates [1], [2], [16] and humans [4], [17], which are supposed to be associated with numerous cognitive functions, such as feature representation [7], [11], [13], signal routing [1], [15], [18], selective attention [1], [2], [17], memory [7], [8], [16] and fear behavior [6], [12].

The associate editor coordinating the review of this manuscript and approving it for publication was Chee Keong Kwoh.

Neuronal oscillatory phase, either for individual neurons or neuronal groups, has been suggested to underlie cognitive functions correlated with feature coding, information routing and behavior performance. For feature coding, a gamma cycle hypothesis advocates that stimulus property, excitatory input and the amplitude of neuronal excitation can be encoded into spike phases [19]. In visual cortex, spike phase provides analog representation of naturalistic movie stimuli [20] and neuronal excitation induced by stimulus orientation [21]. Besides, oscillatory phase provides a coding scheme for spatial location in hippocampus [22], olfactory activation information in olfactory bulb [11], natural sound stimulus in auditory cortex [23] and memorized objects in prefrontal cortex [24]. In computational studies, stimulus strength and excitatory inputs [25], as well as stimulus-related information about input differences [26] can be represented by gamma phases. With regard to information routing, the relative phase in pulvinar can not only modulate

cortical communication, but also determine the directionality of the communication [1], [27]. In addition, the phase difference between neuronal circuits can be utilized to set up or abolish information transfer [28]. With respect to behavior performance, different oscillatory phases bring about distinct behavior performance in the tasks of target detection [29] and letter recognition [30]. Besides, food feeding behaviors in mice can make hypothalamus neurons fire at distinct phases [5].

The oscillatory phase can be represented by spike-LFP (Local Field Potential) phase [21]. Whereas phase synchronization, reflecting phase similarity and precision of neuronal synchronization, can be quantified by a PPC (Pairwise Phase Consistency) method [31], [32]. However, both the spike-LFP phase and the PPC method are generally related to individual neurons. The spike-LFP phase denotes the phase for a spike time point of an individual neuron relative to its surrounding LFP oscillations [32], hereinafter called point spike-LFP phase. The PPC method is defined for measuring the consistency of point spike-LFP phases across spikes of an individual neuron [32].

For individual neurons, the oscillatory phase has been suggested to have quantifiable relationships with neuronal excitation and synaptic input. A gamma cycle hypothesis proposes that stronger external inputs and larger amplitude of excitation for a pyramidal neuron result in earlier spike phases [19]. In visual cortex, the spike-LFP phase of an individual neuron obtains lower values upon preferred orientations and stronger neuronal activations [21]. In hippocampus, when a rat moves into the place field of a given neuron, the excitatory drive representing spatial information is increased, which gives rise to earlier and earlier theta phases [19], [22]. In a computational model, a spike phase of a single neuron shifts from the later to the earlier part in oscillatory cycle as the driving current is increased [25]. For an individual neuron in another computational model, the phase of its firing is decreased when the amplitude of the sinusoidal input is increased [33]. In a simulation, the oscillatory phase of individual neurons decreases monotonically as a function of neuronal excitation and input strength for relatively strong oscillations [34].

Individual neurons are commonly known to make significant contributions to cognitive capacities, for instance, encoding orientation features [35], spectrotemporal auditory properties [36], and high-order substances in images [37], [38]. However, the interconnectivity of individual neurons, both locally and with long-range, is highly inclined to population coding [38]. Besides, a unified perception of an object generally needs to bind various disparate features together [39], commonly under Gestalt psychophysical principles [40], which tends to require involvement of multiple individual neurons. Moreover, it also uncommon for an individual neuron to be activated only by a single stimulus or stimulus feature [38], [41].

Neuronal groups are sometimes referred to as neuronal assemblies, which are supposed to provide a flexible mechanism for cognitive processing. In visual cortex, high-order stimulus properties are suggested to be represented by oscillating neuronal assemblies [42]–[44]. In antennal lobe, olfactory information is encoded by specific assemblies of coherently oscillating neurons [13]. In hippocampus, each moment in time is characterized by the activity of a particular assembly of neurons [14]. In hypothalamus, food feeding behavior is modulated by organization of functional neuronal groups through gamma oscillations [5].

More specially, a variety of evidences indicate that neuronal groups have a competitive advantage over individual neurons in cognitive dynamics. In cat's visual cortex, cooperative synchronized assemblies support better orientation discrimination than found in individual responses [45]. In rat's hippocampus, spatial distances are represented by temporal correlation of place cell pairs, which could be induced by independent neurons or cell assemblies. The temporal correlation is stronger by cell assemblies than by independent neurons [46]. In addition, a computational simulation and its corresponding neurophysiological recording demonstrate the coherence for multi-unit activity is larger than the one for single-unit activity [47]. Another computational investigation illustrates that a flexible routing of information is carried out by means of neuronal populations rather than by individual neurons, on account of individual neurons firing irregularly and sensitive to Poisson-like noise [48].

In view of the facts above, despite the contributions of individual neurons, the function of neuronal assemblies and the superiority of neuronal groups have explicitly suggested that group coding is inevitable and necessary [38]. However, thus far, the point spike-LFP phase for oscillatory phase, the PPC method for phase synchronization, and the relationship quantification for oscillatory phase are primarily for individual neurons. Therefore, how to represent oscillatory phase and phase synchronization for neuronal groups? What are the relationships of oscillatory phase with neuronal excitation and input strength for neuronal groups? Do neuronal groups still have an advantage over individual neurons?

The primary purpose of this paper was to investigate oscillatory phase and phase synchronization for neuronal groups, and quantify the relationships of the oscillatory phase with neuronal excitation and input strength (Fig. 1(a)). Importantly, we carried out a similar investigation for individual neurons, drew comparisons between the two cases, and guaranteed whether the group case was superior to the individual case or not. With regard to oscillatory phase, we proposed a new spike-LFP phase method for individual neurons and neuronal groups, which was based on vector addition of point spike-LFP phases, as opposed to on the basis of averaging the point spike-LFP phases directly. With respect to phase synchronization, we proposed a PPCG (Pairwise Phase Consistency for Group) method to quantify phase coincidence and the strength of neuronal synchronization for neuronal groups. As for individual neurons, we utilized a point-field PPC $\hat{P}_2$ measure [32], referred to here as PPC2 for short, which is a refined version of the PPC approach [31].

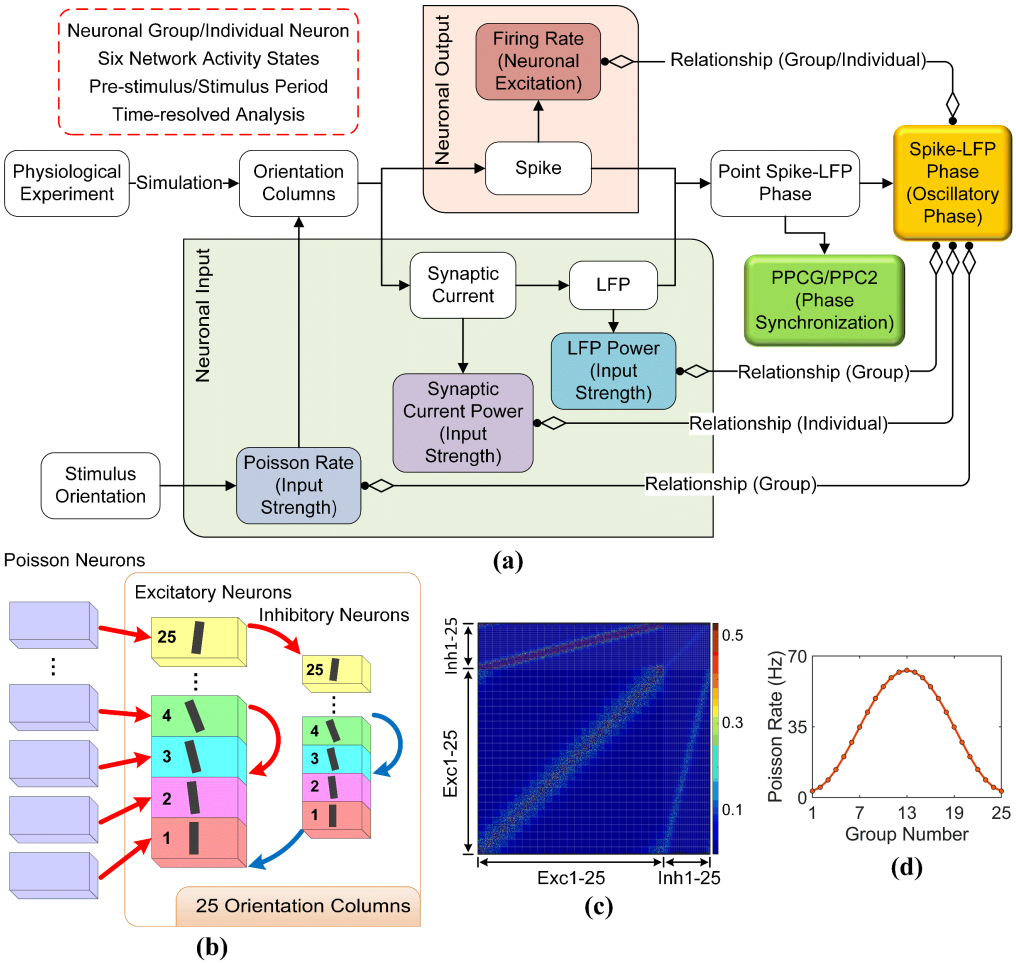

FIGURE 1. Model Overview and Network Framework. (a) Overview of computational model. Base on physiological experiments and a simulation of orientation columns, we primarily investigate oscillatory phase and phase synchronization, as well as relationships of the oscillatory phase with neuronal excitation and input strength for both neuronal groups and individual neurons. Then we guarantee if neuronal groups have an advantage over individual neurons in the relationship quantifications. (b) Framework of neuronal network. On the left side are 25 groups of Poisson neurons, and on the right side are 25 orientation columns, each of which is comprised of a group of excitatory and inhibitory neurons. Black bars with different directions denote preferred orientations for the relevant orientation columns. Red and blue arrows represent excitatory and inhibitory synaptic connectivity respectively. (c) Matrix of connection weight within 25 orientation columns. Exc1-25 depicts excitatory neurons from the 1st column to the 25th column, with Inh1-25 for the case of inhibitory neurons. A color bar indicates the weight value of the synaptic connectivity. (d) Poisson rate of 25 Poisson groups.

The spike-LFP phase provided an indirect measurement between neuronal output and neuronal input (Fig. 1(a)), because an LFP signal was brought about by aggregated synaptic activities of a pool of nearby neurons [32]. For neuronal output, the neuronal excitation was characterized by neuronal firing rate for both individual neurons and neuronal groups. As for neuronal input, the input strength was modeled by synaptic current power for individual neurons, as well as LFP power and Poisson rate for neuronal groups. The experimental simulation and subsequent theoretical analysis were primarily carried out according to a physiological experiment [21] and on the basis of orientation columns, which were approximately constructed by a spike neural network. Besides, in order to obtain independent and comparative investigations, we introduced six network activity states modulated by Gaussian noise [49], a pre-stimulus period with no input stimulus, and a stimulus period with external input of stimulus orientation. Furthermore, a time-resolved analysis with a sliding window was also implemented for quantifying the evolution of oscillatory phase across trial time.

The main contributions and findings of this work are summarized as follows. Firstly, we proposed a new spike-LFP phase method based on vector addition operation. It was demonstrated in the simulation that the vector addition phase was more appropriate than mean phase to characterize the oscillatory phase. Besides, we also proposed a PPCG method for measuring phase synchronization of neuronal groups. Secondly, we confirmed the existence of gamma oscillations in the neuronal network, in agreement with a series of electrophysiological experiments [5], [15] and numerical models

[26], [50]. Thirdly, the oscillatory phase and phase synchronization for neuronal groups possessed similar properties in comparison to the ones for individual neurons. Fourthly, compatible with individual neurons, the oscillatory phase for neuronal groups decreased monotonically with neuronal excitation and input strength as well. It was consistent with a number of physiological experiments [19], [21], [22] and computational investigations [25], [33], [34]. Last and more importantly, we confirmed that neuronal groups were greatly superior to individual neurons in relationship quantification of oscillatory phase with neuronal excitation and input strength.

II. MATERIALS AND METHODS

A. NETWORK FRAMEWORK AND ORIENTATION PREFERENCE

Cortical columns, an elaboration of excitatory-inhibitory circuits and fundamental units of cortical organization [51], are not only critical for the emergence of neuronal oscillations [52], but also more efficient than computation implemented by the same number of neurons connected randomly [44], [53]. Consequently, we simulated orientation columns in primary visual cortex by means of a spiking neuronal network (Fig. 1(b)). The neuronal network encompassed two compartments, the right of which were 25 orientation columns, and the left were 25 Poisson groups, serving as LGN (Lateral Geniculate Nucleus) and providing external thalamic spike inputs to visual cortex. There were 2500 Poisson neurons in total, 100 for each Poisson group. Each orientation column was composed of two cuboids with the same color, index number and orientation bar, representing 100 excitatory neurons and 25 inhibitory neurons respectively. Altogether, there were 3125 neurons within the 25 orientation columns, 80% of which were excitatory neurons. The ratio of excitatory neurons to inhibitory neurons was in accordance with physiological and computational investigations [50], [54], [55].

Owing to orientation selectivity and bell-shape tuning curve of firing rate with respect to orientation stimulus in visual cortex [56], [57], we consecutively designated the excitatory and inhibitory neurons in each of the 25 orientation columns with a preferred orientation, with $-\pi/2 + \pi\,(i-1)/25$ for the i^{th} column. Consequently, the preferred orientations for the 1^{st} and 25^{th} columns were similar, which elicited a ring topology of orientation preference across columns. Similar analogous tuning curve is also observed in head-direction cells of the postsubiculum [48]. Besides, the neurons in 25 Poisson groups were also appointed with the same preferred orientation as their corresponding orientation columns so as to derive appropriate and reliable external input of spike trains.

B. NEURON MODEL

All neurons throughout this paper were described by a leaky integrate-and-fire neuronal model, modified from [58], the membrane potential evolution of which obeyed the following equation:

$$C_m \frac{dV}{dt} = -g_L\,(V - V_{rest}) + I_{AMPA} + I_{GABA} + I_{bg} + C_m\sigma_n\sqrt{\frac{2}{\tau_n}}\xi\,(t) \quad (1)$$

where C_m was a membrane capacitance, g_L a membrane leak conductance, and I_{bg} a constant background current, utilized to maintain minimal neuronal activity and simulate spontaneous activity in cerebral cortex. The term $\xi\,(t)$ denoted a normalized Gaussian white noise [49], τ_n represented a time constant of the Gaussian noise and σ_n was adopted to regulate neuronal network activity state. When a membrane potential V crossed a threshold potential V_{thres}, an action potential was generated, which propagated to all its connected neurons. Then the membrane potential was reset to a resting potential V_{rest} and remained shunted for a refractory period T_{ref}. The synapses were conductance-based and the synaptic currents were modulated by excitatory (AMPA) and inhibitory (GABA) receptors, the dynamics of which were as follows:

$$I_{AMPA} = g_{AMPA}\,(V_E - V) \quad (2)$$

$$I_{GABA} = g_{GABA}\,(V_I - V) \quad (3)$$

V_E and V_I were excitatory and inhibitory reversal potentials respectively. Whenever a neuron received an action potential, its conductance was increased accordingly, with $g_{AMPA} = g_{AMPA} + \Delta g_{AMPA}$ for the excitatory synapse and $g_{GABA} = g_{GABA} + \Delta g_{GABA}$ for the inhibitory synapse correspondingly. Both Δg_{AMPA} and Δg_{GABA} were determined by a connection weight to be elucidated in the next section. Otherwise, the conductance of the neuron evolved according to the equations below:

$$\frac{dg_{AMPA}}{dt} = -\frac{g_{AMPA}}{\tau_{AMPA}} \quad (4)$$

$$\frac{dg_{GABA}}{dt} = -\frac{g_{GABA}}{\tau_{GABA}} \quad (5)$$

where τ_{AMPA} and τ_{GABA} were excitatory and inhibitory decay time constants.

C. SYNAPTIC CONNECTIVITY

Topographic specificity, functional specificity, together with cell-type specificity constitute the major determinants of cortical connectivity [59], [60]. The synaptic connections between Poisson groups and their corresponding orientation columns were one-to-one and feedforward, with constant and identical connection weight W_f (Fig. 1(b)). The probability of the synaptic connection was $\varepsilon = 20\%$. The feedforward connectivity established a wild and initial orientation preference, on the basis of feedforward models proposing that orientation selectivity is simply generated by thalamic inputs from LGN to visual cortex [59], [60].

The connection weight between interconnected neurons within 25 orientation columns depended on feature

discrepancy of preferred orientation between presynaptic and postsynaptic neurons.

$$W_{ij} = We^{\beta[\cos(2(\theta_{pre}-\theta_{post}))-1]} \quad (6)$$

where θ_{pre} and θ_{post} represented the preferred orientations for the presynaptic and postsynaptic neurons respectively. The parameter W had four variables: W_{EE}, W_{EI}, W_{IE}, W_{II}, denoting basic connection weights from excitatory to excitatory, excitatory to inhibitory, inhibitory to excitatory, inhibitory to inhibitory neurons respectively. Besides, the probability of the recurrent synaptic connection was also $\varepsilon = 20\%$. Particularly, in order to obtain an appropriate excitatory-inhibitory balance in the neuronal network, W_{IE} was configured with a larger value than W_{EI} on account of relatively small number of inhibitory neurons [50], [61], [62]. It has been proposed by feedback and recurrent models that orientation selectivity is amplified by excitatory intracortical interconnections and inhibitory interactions [56], [63]. Accordingly, the recurrent connectivity within the 25 orientation columns in our simulation reinforced the orientation preference.

As illustrated Fig. 1(c) was a matrix of connection weight within 25 orientation columns obtained in our simulation. The matrix consisted of four main compartments or matrices, representing connection weights from inhibitory (Inh1-25) to excitatory (Exc1-25), inhibitory to inhibitory, excitatory to excitatory, excitatory to inhibitory neurons respectively. For small matrices along four diagonal lines of the four main compartments, the connection weights obtained the highest values because neurons within an orientation column possessed the same orientation preference. For small matrices nearby the four diagonal lines, the connection weights derived the secondly highest values due to similar orientation preference. As for other small matrices, the connection weights decayed substantially. This distribution of connection weights was primarily attributable to the increasing difference of orientation preference and uprising distance between orientation columns. It was in tune with the evidence that the probability of synaptic connectivity declines exponentially with the distance between neurons or regions [50], [64]. Besides, the synaptic connection weights were kept constant in this simulation for simplicity of network design and efficiency of computation. However, we could equally acquire similar neuronal activities and network dynamics in the case of varying synaptic connection strengths.

D. SIMULATION AND DATA RECORDING

In our simulation, there were six network activity states, which were brought about by six levels of Gaussian white noise (state1 ($\sigma_n = 0.5$ mV), state2 ($\sigma_n = 1.0$ mV), state3 ($\sigma_n = 1.5$ mV), state4 ($\sigma_n = 2.0$ mV), state5 ($\sigma_n = 2.5$ mV) and state6 ($\sigma_n = 3.0$ mV)) [65]–[67]. However, we could equivalently obtain the network activity states by other categories of noise or by other parameters such as synaptic time constant, synaptic strength or periodic external input [48]. We conducted 20 trials for each network activity state, and ultimately derived 120 trials in total for the whole simulation. For each trial, there were a 500 ms pre-stimulus period and a 1500 ms stimulus period. During pre-stimulus period, only Poisson spike inputs with a lower rate F_{bg} and a constant background current I_{bg} were delivered to the neuronal network so as to maintain minimal neuronal activity and simulate the spontaneous activity in cerebral cortex [68]. During stimulus period, we continuously imported a constant stimulus orientation, with a degree of $-\pi/50$, to simulate drifting gratings in electrophysiological experiments. Typically, the orientation of input stimulus was identical to the preferred orientation of the 13th orientation column.

From bottom to top in Fig. 2(a) was the distribution of 25 orientation columns consecutively. For each column, we selected 20 nearby excitatory neurons and recorded their spike times, excitatory synaptic currents I_{AMPA}, inhibitory synaptic currents I_{GABA}, as well as their background currents I_{bg} for 120 trials of all six network activity states. It corresponded to a microelectrode recording site in electrophysiological experiments. Besides, it also satisfied the minimal size requirement of a cell assembly (10^1-10^2 neurons) [38]. Every 20 excitatory individual neurons constituted a neuronal group, which meanwhile gave rise to an LFP channel. Overall, there were 500 individual neurons, 25 neuronal groups, 25 LFP channels and 25 simulation sites recorded in this simulation. The spike sample frequency was 10000 Hz, and the sample frequency for LFP and synaptic current was 1000 Hz. In addition, if not mentioned otherwise, the recording data of the first 120 ms and 250 ms for pre-stimulus and stimulus periods was discarded owing to response onset transient effect [21].

Additionally, a Python based simulator for spiking neural network, named Brian [69], was utilized in our simulation for column network construction, experiment simulation and data recording. The simulation adopted a Euler integration method, with a time step of 0.1 ms. Besides, a MATLAB toolbox, namely FieldTrip [70], and its Spike package [21] were employed for subsequent theoretical computation and spectral analysis. Moreover, the relevant statistical analysis was carried out with the help of SPSS and EXCEL. Furthermore, all parameters encountered in this paper were configured according to Table 1.

TABLE 1. Default parameter configuration.

Parameter	Value	Parameter	Value
C_m	250 pF	g_L	10 nS
I_{bg}	270 pA	σ_n	0.5/1.0/1.5/2.0/2.5/3.0 mV
τ_n	25 ms	V_{thres}	-45 mV
V_{rest}	-65 mV	T_{ref}	5 ms
V_E	0 mV	V_I	-75 mV
τ_{AMPA}	5 ms	τ_{GABA}	10 ms
W_f	0.15	ε	20%
β	5	W_{EE}	0.29
W_{EI}	0.2	W_{IE}	0.53
W_{II}	0.1	F_{max}	30 Hz
F_{bg}	3 Hz	R	1.0 MΩ

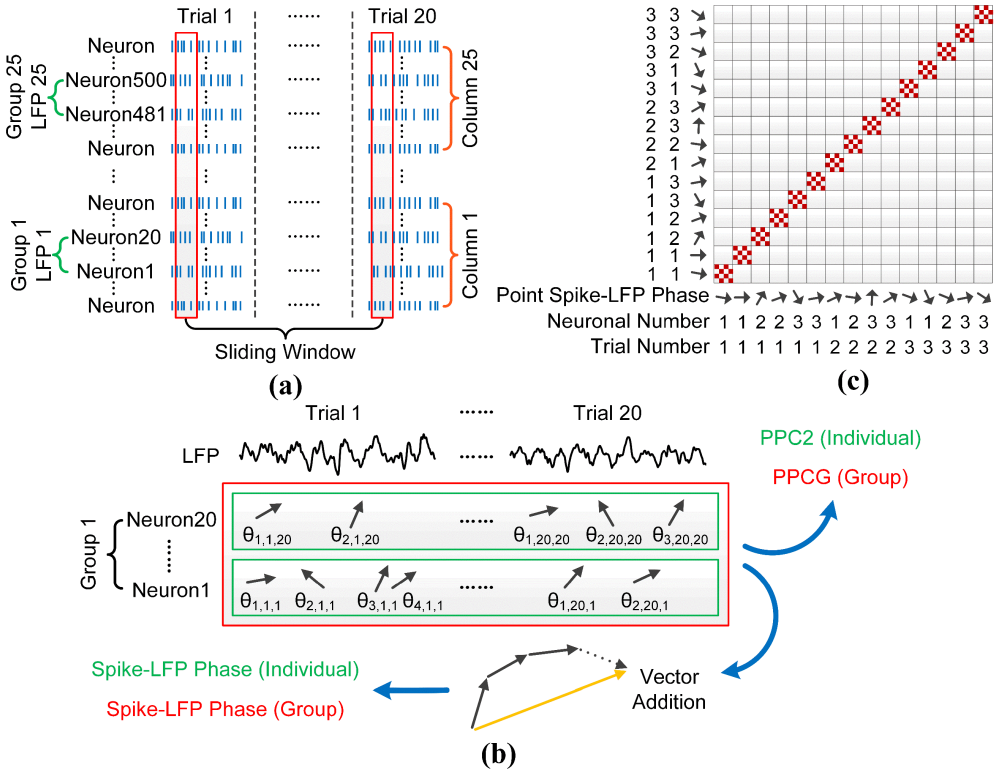

FIGURE 2. Simulation Overall and Computations of Spike-LFP Phase and PPCG. (a) Simulation overall. In each orientation column, there is a neuronal group, composed of 20 excitatory individual neurons, which meanwhile bring about an LFP channel. The red rectangles are sliding windows for time-resolved analysis. (b) Computations of spike-LFP phase, PPCG and PPC2. A point spike-LFP phase $\theta_{k,m,n}$, depicted by an arrow, corresponds to a spike of a given neuron. The spike-LFP phase is computed based on vector addition of point spike-LFP phases across trials and neurons. The spike-LFP phase and PPC2 for an individual neuron are based on the point spike-LFP phases within a green rectangle. The spike- LFP phase and PPCG for a neuronal group are on the basis of the point spike-LFP phases within a red rectangle. (c) Illustration of PPCG Method. There are point spike-LFP phases from 3 neurons and 3 trials in a neuronal group. They are represented by arrows and duplicated on the x-axis and y-axis. The PPCG method is based on dot product operation of pairs of the point spike-LFP phases. The dot product of a point spike-LFP phase with itself always equals one and therefore is ignored in the PPCG computation, which is represented by diagonal squares with red patterns.

E. INPUT STRENGTH

1) POISSON RATE

The Poisson rate P_{rate} was primarily determined by the feature difference between the preferred orientation θ_{pref} of a Poisson neuron and the stimulus orientation θ_{stim} imported in the simulation, with the equation inspired from [48].

$$P_{rate} = \left[\cos\left(2\left(\theta_{pref} - \theta_{stim}\right)\right) + 1\right] F_{max} \tag{7}$$

where F_{max} represented a maximal rate. The distribution of the Poisson rate for 25 Poisson groups was portrayed in Fig. 1(d). The 13th Poisson group obtained the highest Poisson rate because its preferred orientation was identical to the input stimulus orientation.

2) SYNAPTIC CURRENT POWER

For an excitatory neuron, we described the synaptic current $I_{current}$ as the sum of excitatory synaptic current I_{AMPA} and constant background current I_{bg}.

$$I_{current} = I_{AMPA} + I_{bg} \tag{8}$$

$$Power_{current} = \frac{\sum_{m=1}^{M}\left\{10 \times \log_{10}\left[pwelch\left(I_{current}\right)\right]\right\}}{M} \tag{9}$$

Both the parameter I_{AMPA} and I_{bg} were the excitatory inputs for the excitatory neuron. The synaptic current power $Power_{current}$, for individual neurons, was quantified by a method of Welch's power spectral density estimate, the MATLAB function of which was denoted by the term *pwelch*. A default Hamming window was used to obtain eight segments of $I_{current}$, and with a default overlap between the segments. The parameter $M = 20$ was the trial number in a network activity state.

3) LFP POWER

We formulated LFP data as the sum of absolute values of excitatory synaptic current I_{AMPA}, inhibitory synaptic current I_{GABA} and constant background current I_{bg} acting upon a group of nearby excitatory neurons [71], with Equation (10) modified from [50], [62].

$$LFP = R\left[\sum_{n=1}^{N}\left(\left|I_{AMPA}\right| + \left|I_{GABA}\right| + \left|I_{bg}\right|\right)\right] \tag{10}$$

$$Power_{LFP} = \frac{\sum_{m=1}^{M} \left\{10 \times \log_{10}\left[pwelch\left(LFP\right)\right]\right\}}{M} \tag{11}$$

The term R represented the resistance of a typical microelectrode in electrophysiological experiments. The parameter I_{AMPA} accounted for both the external thalamic current from Poisson spike train and excitatory recurrent synaptic current within the 25 orientation columns. Whereas I_{GABA} merely manifested inhibitory recurrent synaptic current within the 25 columns. The term $N = 20$ expressed the neuronal number in a neuronal group, which satisfied the lower bound on the size of cell assemblies [38]. The LFP signal was bandpass filtered with 0.7-170 Hz. The LFP power $Power_{LFP}$, for neuronal groups, was also achieved by virtue of the Welch's power method. We adopted a default Hamming window to derive eight segments of LFP signals and with a default overlap between the segments. The parameter M described the trial number in a network activity state and equaled 20.

F. NEURONAL EXCITATION

The neuronal excitation is quantified by neuronal firing rate for both individual neurons and neuronal groups. We defined $N_{m,n}$ as the spike count of the nth neuron in the mth trial, $\mathrm{n} \in \{1, \cdots, N\}$, $\mathrm{m} \in \{1, \cdots, M\}$, where $N = 20$ was the neuronal number in a neuronal group, and $M = 20$ the trial number in a network activity state.

$$FRate_{idv} = \frac{\sum_{m=1}^{M} N_{m,n}}{MT_{dur}} \tag{12}$$

$$FRate_{gp} = \frac{\sum_{n=1}^{N}\sum_{m=1}^{M} N_{m,n}}{NMT_{dur}} \tag{13}$$

where $FRate_{idv}$ and $FRate_{gp}$ denoted the neuronal firing rates for an individual neuron and a neuronal group respectively. The term T_{dur} described a duration in a trial, with 500 ms for pre-stimulus period, and 1500 ms for stimulus period.

G. SPIKE-LFP PHASE

For a spike of a given neuron, 24 LFP segments from other 24 orientation columns were cut out, except the one within the same column. The center of each segment was aligned with the spike time. The length of LFP segment was varied for different frequencies, with five cycles per frequency. Each LFP segment was multiplied by a Hanning window. Then we implemented Discrete Fourier Transform and obtained the spike-triggered LFP spectrum $X_i\left(f\right)$ for a certain frequency, through Equation (14) [21].

$$X_i\left(f\right) = \sum_{t}^{T} w\left(t\right) x_i\left(t\right) e^{-2\pi jft} \tag{14}$$

$$\bar{X}_i\left(f\right) = \frac{1}{24}\sum_{s=1}^{24} \frac{X_i^s\left(f\right)}{\left|X_i^s\left(f\right)\right|} \tag{15}$$

$$\Theta_i = angle\left(\bar{X}_i\left(f\right)\right) \tag{16}$$

where $x_i\left(t\right)$ was the time series of an LFP segment centered around the ith spike, and $w\left(t\right)$ was the Hanning window. We averaged the outcomes across the 24 LFP channels by means of Equation (15) [21], through which the magnitude of the spike-triggered LFP spectrum was normalized and ignored. The term $X_i^s\left(f\right)$ manifested the spike-triggered LFP spectrum for the sth LFP channel relative to the ith spike of the given neuron. Then a point spike-LFP phase Θ_i could be easily acquired by Equation (16), where the term *angle* was a MATLAB function for computing the phase angle of complex data.

The term $\bar{X}_i\left(f\right)$ was a complex number. Then it was categorized into $\bar{X}_{k,m,n}\left(f\right)$ according to its neuronal number and trial number, where $\mathrm{n} \in \{1, \cdots, N\}$, $\mathrm{m} \in \{1, \cdots, M\}$, $\mathrm{k} \in \left\{1, \cdots, N_{m,n}\right\}$. $N = 20$ was the neuronal number in a neuronal group, $M = 20$ the trial number in a network activity state, $N_{m,n}$ the spike count of the nth neuron in the mth trial. The spike-LFP phase for an individual neuron Θ_{idv} and the spike-LFP phase for a neuronal group Θ_{gp} could be precisely established by virtue of Equations (17) and (18) respectively.

$$\Theta_{idv} = angle\left(\frac{\sum_{m=1}^{M}\sum_{k=1}^{N_{m,n}} \bar{X}_{k,m,n}\left(f\right)}{\sum_{m=1}^{M} N_{m,n}}\right) \tag{17}$$

$$\Theta_{gp} = angle\left(\frac{\sum_{n=1}^{N}\sum_{m=1}^{M}\sum_{k=1}^{N_{m,n}} \bar{X}_{k,m,n}\left(f\right)}{\sum_{n=1}^{N}\sum_{m=1}^{M} N_{m,n}}\right) \tag{18}$$

Importantly, the spike-LFP phase for individual neurons and neuronal groups in this paper was based on vector addition of point spike-LFP phases, instead of on the basis of averaging the point spike-LFP phases directly. For the spike-LFP phase of an individual neuron, the vector addition operation was performed for the point spike-LFP phases within a green rectangle in Fig. 2(b). Whereas the point spike-LFP phases within a red rectangle were used for computing the spike-LFP phase of a neuronal group.

H. PAIRWISE PHASE CONSISTENCY FOR GROUP PPCG

For an individual neuron, we adopted a PPC2 method [32] to quantify phase consistency or phase synchronization, which depended on the point spike-LFP phases within a green rectangle in Fig. 2(b). On the basis of the PPC method [31], [32], we proposed a new method of pairwise phase consistency for group, referred to here as PPCG, to measure the precision of phase synchronization for neuronal groups.

First of all, a point spike-LFP phase Θ_i was classified into $\Theta_{k,m,n}$ according to its neuronal number and trial number, wherein $\mathrm{n} \in \{1, \cdots, N\}$, with $N = 20$ representing the neuronal number in a neuronal group, $\mathrm{m} \in \{1, \cdots, M\}$, with $M = 20$ describing the trial number in a network activity state, and $\mathrm{k} \in \left\{1, \cdots, N_{m,n}\right\}$, with $N_{m,n}$ denoting the spike count of the nth neuron in the mth trial. Then we defined a vector of $U_{k,m,n} \equiv \left(\cos\left(\Theta_{k,m,n}\right), \sin\left(\Theta_{k,m,n}\right)\right)$ to represent the point spike-LFP phase $\Theta_{k,m,n}$. Ultimately, the PPCG method was defined by Equation (19) (As shown at the bottom of the next page). The symbol $\cdot$ was an operator of dot product. The term $\mathcal{M}$ was defined as $\left\{m \in \{1, \cdots, M\}; N_{m,n} > 0\right\}$, in which $|\mathcal{M}|$ was the trial number with at least one spike. $L = \sum_{n=1}^{N}\sum_{m=1}^{M} N_{m,n}$ embodied the total spike number within a neuronal group. The computation of PPCG was

based on the point spike-LFP phases within a red rectangle in Fig. 2(b). Besides, the sextuple summation in the PPCG equation implemented the dot product of all pairs of point spike-LFP phases across neurons and trials within a neuronal group except the one with itself. As visible in Fig. 2(c), the diagonal squares with red patterns, indicating combinations of a point spike-LFP phase with itself, were ignored in the dot product computation. Because the dot product of a point spike-LFP phase with itself always equaled one and did not contribute to the PPCG statistic, which was eliminated by the subtraction of L.

III. RESULTS

A. NETWORK ACTIVITY AND POWER SPECTRUM

During stimulus period, the spike raster of Poisson (Pois) neurons had a higher spike density in its middle region (Fig. 3(a)), compatible with the distribution of Poisson rate across Poisson groups (Fig. 1(d)). The instantaneous firing activities of both excitatory (Exc) and inhibitory (Inh) neuronal populations exhibited robust oscillation and collective rhythmogenesis, while their individual neurons discharged sparsely and irregularly at lower rates (Fig. 3(a1)). This characteristic of irregular spiking at individual neuronal level and rhythmic oscillation at group level are generally observed in vivo [3] and computational studies [48], [50]. Besides, the inhibitory neurons, with relatively sparse spike raster and small number, compensated themselves with strong synaptic conductance to obtain excitatory-inhibitory balance in the neuronal network [50].

In addition to oscillatory activities in spike raster, there were also rhythmic oscillations observed in LFP signal for neuronal groups Fig. 3(b, c1) and in synaptic current signal for individual neurons (Fig. 3(c2)). The two types of oscillatory signals varied in phase across trial time and were also consistent with their corresponding spike raster, all within gamma band frequency. Moreover, the oscillation phenomenon was also encountered in neuronal firing rate signal for individual neurons, however, at a much lower frequency (Fig. 3(c3)). Experiments with pharmacological and optogenetic manipulation of interneurons as well as computational simulations have demonstrated that GABA receptor mediated synaptic inhibition and recurrent interaction between excitatory and inhibitory neurons are responsible for generating neuronal oscillations [19], [38], [44], [72]. When we gradually increased the parameter σ_n of Gaussian white noise, the network activity state switched from robust oscillation to weak oscillation or non-oscillation (Fig. 3(a)).

As demonstrated in Fig. 3(a1, b), it seems as if there existed a time sequence for both oscillatory spike raster and LFP signals across different orientation columns during stimulus period. The oscillation of spike raster emerged firstly in the 13^{th} orientation column, and then appeared in the two-side columns successively. Similar phenomenon was encountered in the LFP signals as well, with the 13^{th}, the 7^{th} and the 1^{st} LFP signals fluctuating roughly in succession. In addition, it has been observed that neurons are more likely to spike near the troughs of LFP oscillations because of the minimal inhibition during this interval [50]. Consequently, the time sequences of oscillatory spike raster and LFP signals, along with the specificity of spike occurrence may lay the foundation for producing various oscillatory phases and diverse strengths of phase synchronization.

For spectral analysis, the appearances of synaptic current power and LFP power were consistent with a number of experimental and simulating evidences (Fig. 3(d)) [26], [50], [67], [73]. Besides, it has been recognized that the frequency of oscillations can be modulated by several parameters, including inhibitory decay time constant [50], [62], [74], stimulus contrast [26], [62], [75] and strength of excitatory and inhibitory inputs [44]. The variation of the stimulus contrast can be achieved by modulating the rate of external spike train [62], [71]. Owing to various Poisson rates for different orientation columns and diverse σ_n values for different network activity states, there existed a certain degree of shifts in peak frequency of both synaptic current power and LFP power across orientation columns, network activity states and trial periods (Fig. 3(d, e)). Furthermore, it has been established in a physiological experiment that gamma coherence can occur despite large changes in frequency, and neuronal communication does not require a fixed frequency [73]. Another experimental evidence indicates that phase coherence between LFP signals obtains the largest value close to the peak frequency of spectral power [52], [62]. Consequently, the subsequent quantifications of spike-LFP phase, PPC2 and PPCG values, as well as synaptic current power and LFP power were based on the peak frequencies of LFP power for different orientation columns, as illustrated in Fig. 3(e).

B. SPIKE-LFP PHASE

During pre-stimulus period in state1, spike-LFP phases were considerably similar across both individual neurons and neuronal groups (Fig. 4(a, b)). They were comparatively consistent and highly concentrated in each orientation column (Fig. 4(c)). From state1 to state6 during this period, the spike-LFP phases shifted and scattered more and more extensively, especially for individual neurons in state6.

During stimulus period in state1, spike-LFP phases for individual neurons from middle orientation columns,

$$PPCG = \frac{\left[\sum_{n=1}^{N}\sum_{t=1}^{N}\sum_{m\in M}\sum_{s\in\mathcal{M}}\sum_{k=1}^{N_{m,n}}\sum_{i=1}^{N_{s,t}}\left(U_{k,m,n}\cdot U_{i,s,t}\right)\right] - L}{L\left(L-1\right)} \tag{19}$$

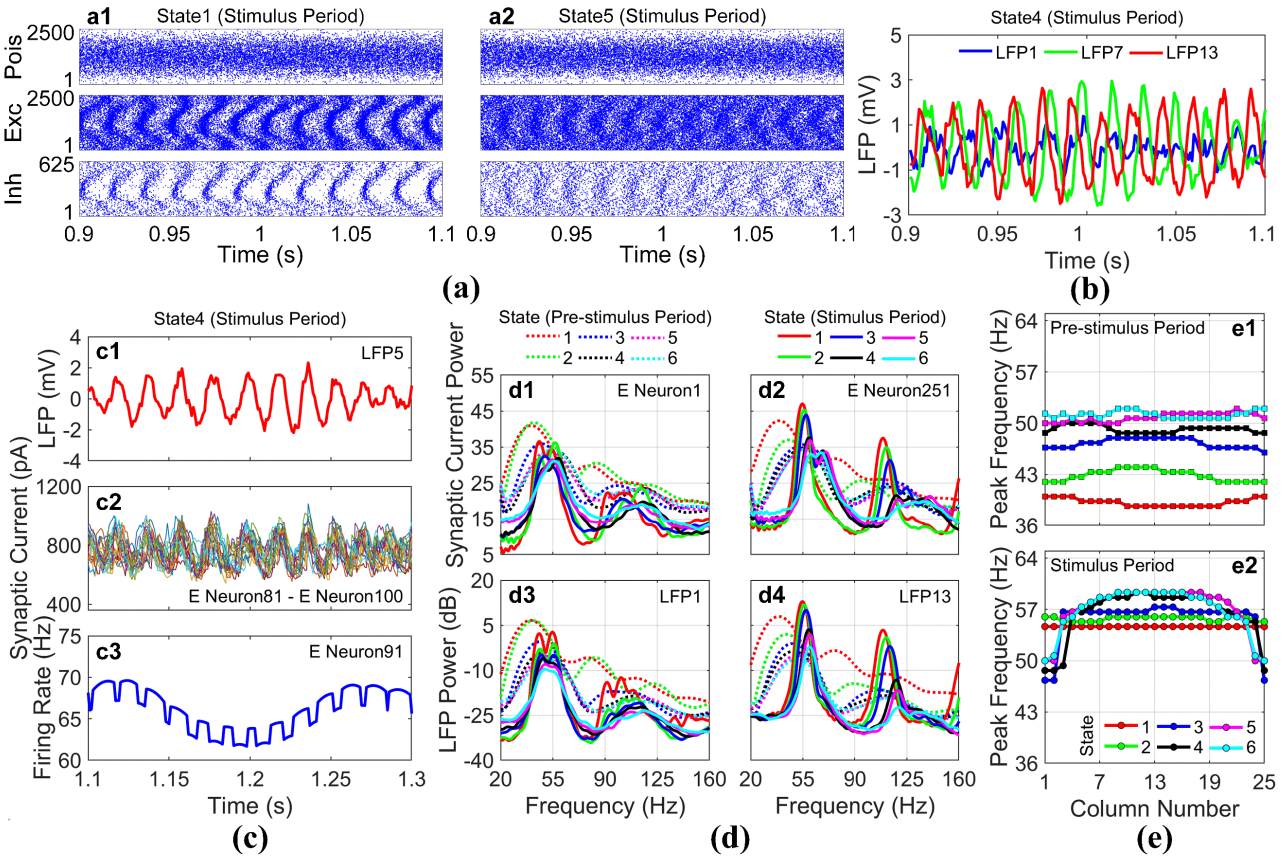

FIGURE 3. Neuronal Activity and Power Spectrum. (a) Spike raster of all neurons in a 200 ms interval in state1 (a1) and state5 (a2) during stimulus period. Pois denotes Poisson neuron, Exc excitatory neuron and Inh inhibitory neuron. (b) Three LFP signals from the 1st, the 7th, the 13th orientation columns in a 200 ms interval in state4 during stimulus period. LFP1 denotes a LFP signal from the 1st orientation column. (c) Neuronal signals from the 5th orientation column in state4 during stimulus period, including a LFP signal (c1), synaptic current signals (c2) and a neuronal firing rate signal (c3). E neuron81 represents the 81th excitatory neuron. Excitatory neurons between 81 and 100 belong to the 5th orientation column, with the E neuron91 in the middle of the column. (d) Synaptic current power (d1 and d2) and LFP power (d3 and d4) in six network activity states during pre-stimulus and stimulus periods. (e) Peak frequencies of LFP power spectra for 25 orientation columns in six network activity states during pre-stimulus period (e1) and stimulus period (e2).

especially the 13th column, were not only smaller (Fig. 4(a)), but also more concentrated (Fig. 4(c)). Whereas the ones from leftward and rightward columns increased gradually and became increasingly scattered. The spike-LFP phases for neuronal groups possessed a similar tuning curve (Fig. 4(b)). From state1 to state6 during this period, the spike-LFP phases for individual neurons fluctuated more and more vigorously, especially for two-side columns, whereas the ones for neuronal groups became increasingly similar across orientation columns.

The preferred orientations for the middle columns were equal or similar to the orientation of input stimulus, which gave rise to stronger external Poisson inputs and higher neuronal excitations for these columns. However, the two-side columns with divergent preferred orientations came up with smaller Poisson inputs and lower neuronal excitations. The spike-LFP phase depended on the level of neuronal excitation which, in turn, relied primarily on input strength and orientation preference, with stronger input strength leading to smaller oscillatory phase. It was highly consistent with a gamma cycle hypothesis [19], a theta-phase precession phenomenon [22], a gamma-phase shifting study [21], and other computational investigations [25], [33]. Besides, stronger external input was more likely to constrain the spike times to a certain interval of LFP oscillations, thereby resulting in more concentrated spike-LFP phases in the middle columns. Furthermore, it has been recognized that neuronal oscillation is framed by synchronized inhibitory interneurons [19]. Owing to the largest Poisson input and strong synaptic connectivity, the rhythmic synchronization of inhibitory neurons emerged firstly in the 13th orientation column, and then in the leftward and rightward columns consecutively. Consequently, it appears as if there existed a time sequence of synchronized inhibitions and LFP oscillations for 25 orientation columns, which might provide a reasonable account for the generation of spike-LFP phases in sequence for both individual neurons and neuronal groups across orientation columns during stimulus period.

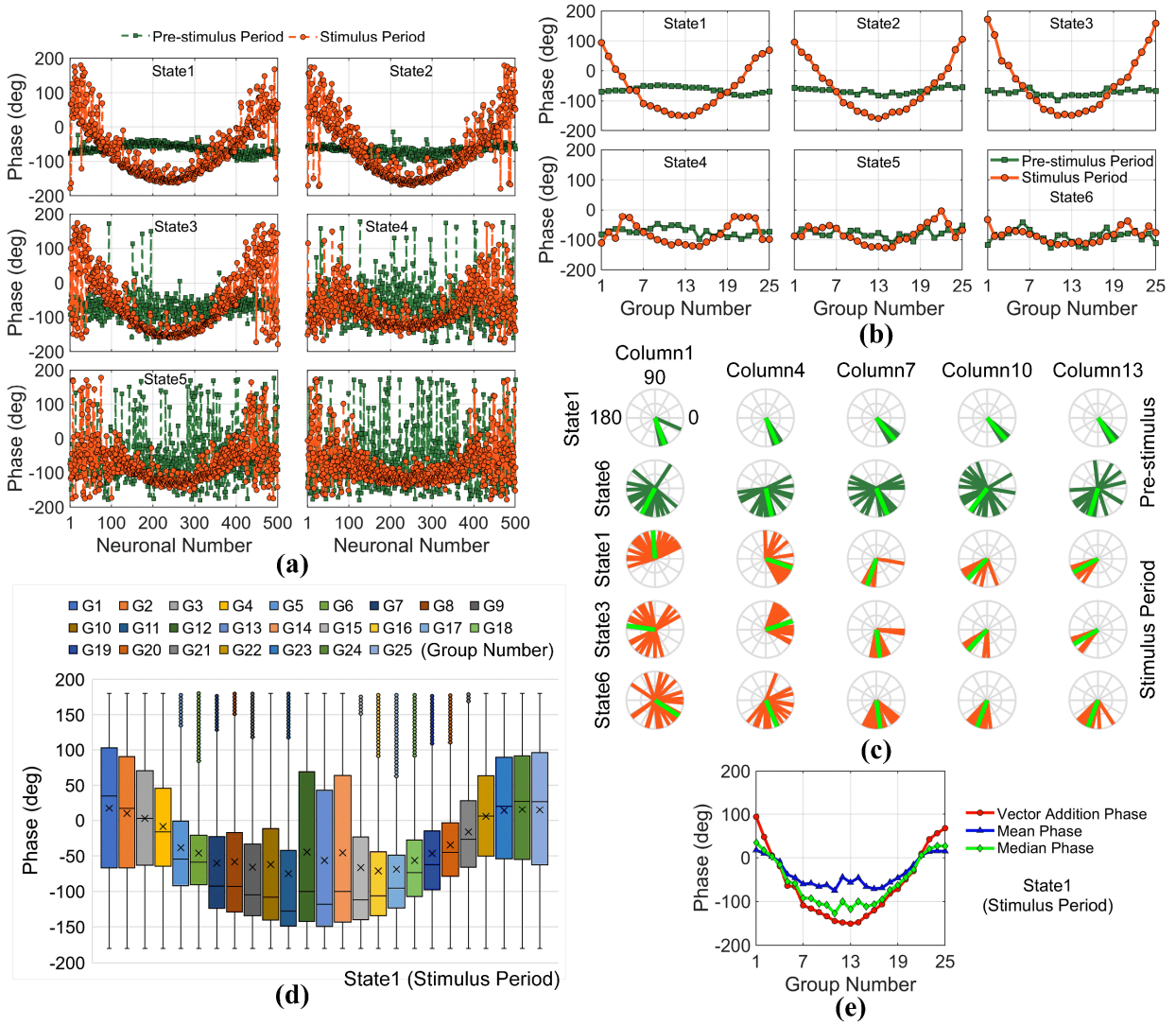

FIGURE 4. Spike-LFP Phase. (a) Spike-LFP phases of 500 individual neurons in six network activity states during pre-stimulus and stimulus periods. (b) Similar to (a), but for spike-LFP phases of 25 neuronal groups. (c) Spike-LFP phases in polar coordinates, with one column for an orientation column and one row for a network activity state. There are 21 spike-LFP phases in each polar coordinates. 20 spike-LFP phases are for individual neurons, with orange bars for stimulus period and blue bars for pre-stimulus period. A green bar denotes a spike-LFP phase for a neuronal group. (d) Box plot of point spike-LFP phases for 25 neuronal groups in state1 during stimulus period. (e) Comparison of different phases. Vector addition phase is utilized to represent the spike-LFP phase in this paper. Mean phase and median phase are statistics of point spike-LFP phases for 25 neuronal groups.

The spike-LFP phase for individual neurons and neuronal groups in this paper was computed by means of vector addition of point spike-LFP phases, instead of averaging the point spike-LFP phases directly. The spike-LFP phase through vector addition operation was referred to here as vector addition phase, whereas the one through averaging method was denoted as mean phase. We also obtained median phase from the point spike-LFP phases for comparison (Fig. 4(e)). As demonstrated in Fig. 4(d) was a box plot of point spike-LFP phases for 25 neuronal groups across 20 trials in state1 during stimulus period. For two-side neuronal groups, the median phase was roughly similar to the mean phase. As for middle neuronal groups, there were wide divergences between the median phase and the mean phase. Besides, the interquartile ranges (IQR) for the middle groups were comparatively large, and the median phase was much closer to the first quartiles (Q1), meaning that the majority of the point spike-LFP phases in the middle groups tended to have smaller values. Take the 13^{th} neuronal group for instance, the relevant statistics were as follows: mean phase: $-56.7°$, median phase: $-117.9°$, vector addition phase: $-151.0°$, Q1: $-149.5°$, IQR: $106.5°$. It was noticed that the median phase was closer to the vector addition phase than to the mean phase. For comparison of all neuronal groups, we utilized a Euclidean distance method to quantify their distances, with $DV = 128.3$, $DM = 156.3$, and $DV < DM$. The term

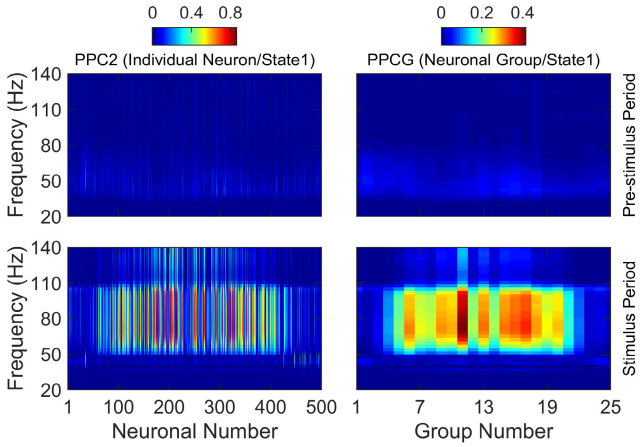

FIGURE 5. PPC2 and PPCG. PPC2 (left panel) for individual neurons and PPCG (right panel) for neuronal groups in state1 during pre-stimulus period (upper panel) and stimulus period (lower panel).

DV represented the Euclidean distance between the vector addition phase and the median phase, and *DM* denoted the one between the mean phase and the median phase. It implied that, in comparison to the mean phase, the vector addition phase was closer to the median phase and therefore more suitable for representing oscillatory phase.

C. PAIRWISE PHASE CONSISTENCY

In this section, phase synchronization was quantified by a PPCG method for neuronal groups and by a PPC2 method for individual neurons. Only the outcome of state1 was exhibited (Fig. 5). The quantification of phase synchronization was thought to provide a mechanistic substrate for implementing cortical communication through CTC (Communication through Coherence) hypothesis [76], [77]. During pre-stimulus period, 25 neuronal groups came up with extremely low and similar PPCG values, so it was with 500 individual neurons with PPC2 values. During stimulus period, the majority of both neuronal groups and individual neurons from middle orientation columns obtained comparatively larger PPCG or PPC2 values, which decreased in two-side columns. It was compatible with physiological experiments that neurons in cortical columns rhythmically synchronized their spike activities upon congruent stimuli [44], [78] and columns coding for related features oscillate with zero phase lag [19], [79]. Besides, the PPCG and PPC2 with higher values were roughly between 55 Hz and 100 Hz, belonging to the range of gamma frequency band. It suggested that gamma oscillations existed in the neuronal network, in agreement with a number of physiological experiments [15], [21], [73] and numerical studies [50], [68].

Owing to mutual and reciprocal connectivity within 25 orientation columns, the middle orientation columns, as a target network, received synaptic inputs from their corresponding Poisson groups, the middle columns themselves and two-side columns. The middle columns, with larger Poisson inputs and strong synaptic connectivity, were more coherence than the two-side columns, which prohibited the two-side columns from being noticed by the target network [80]. Besides, the synaptic inhibition and the balanced excitation and inhibition in the middle columns greatly decreased the resistance of neuron membrane and therefore increased the leakiness of target neurons [33], [80]. Consequently, neurons in the middle orientation columns were more likely to act as coincidence detectors [33], [72], more vulnerable to synchronous inputs, and therefore had higher probability to obtain larger PPCG and PPC2 values.

D. RELATIONSHIP BETWEEN OSCILLATORY PHASE AND NEURONAL EXCITATION

In this section, we primarily investigated the relationship between spike-LFP phase and neuronal excitation, quantified by neuronal firing rate, for both individual neurons and neuronal groups. During pre-stimulus period in each network activity state, the distribution of firing rate for neuronal groups was roughly similar, in spite of a certain degree of variations (Fig. 6(b)). Whereas the one for individual neurons varied considerably, nevertheless similar across orientation columns (Fig. 6(a)). During stimulus period in each network activity state, owing to comparatively larger density of spike raster in middle orientation columns (Fig. 3(a)), both individual neurons and neuronal groups from these columns came up with stronger neuronal excitation and hence larger firing rates, which decreased gradually towards leftward and rightward columns. From state1 to state6, the firing rates for individual neurons and neuronal groups became comparatively larger and larger. In particular, the firing rate tuning curves during stimulus period were not only consistent with the Poisson rate of 25 Poisson groups (Fig. 1(d)), but also in line with the evidence that neuronal firing rate in visual cortex is sensitive to orientation stimulus [56], [60].

Typically, the firing rate was a linear predictor variable, whereas the spike-LFP phase was a circular variable. Therefore, their relationship cannot be investigated appropriately by means of a standard linear regression model, which can only minimize linear errors rather than circular errors. Consequently, we utilized a linear-circular regression model with an arctangent link function, which could map linear predictor variables to circular ones. The equation of the regression model, revised from [21], was as follows:

$$\theta_i = \mu + \alpha \tan^{-1}(\beta Y_i + b) + \varepsilon_i \tag{20}$$

where the term θ_i denoted a spike-LFP phase and Y_i represented a neuronal firing rate for the i^{th} individual neuron or the i^{th} neuronal group. ε_i obeyed a von Mises distribution [81]. The parameter β was the coefficient of regression slope that we attempted to estimate.

With regard to individual neurons, we firstly quantified the relationships for all 500 individual neurons. Only two regression curves with sliding slopes in state1 and state2 could be estimated (Fig. 6(c)). According to Table 2, the estimated regression coefficient β $\{-8.212, -0.427\}$ for the two curves were negative. Unfortunately, the R squared,

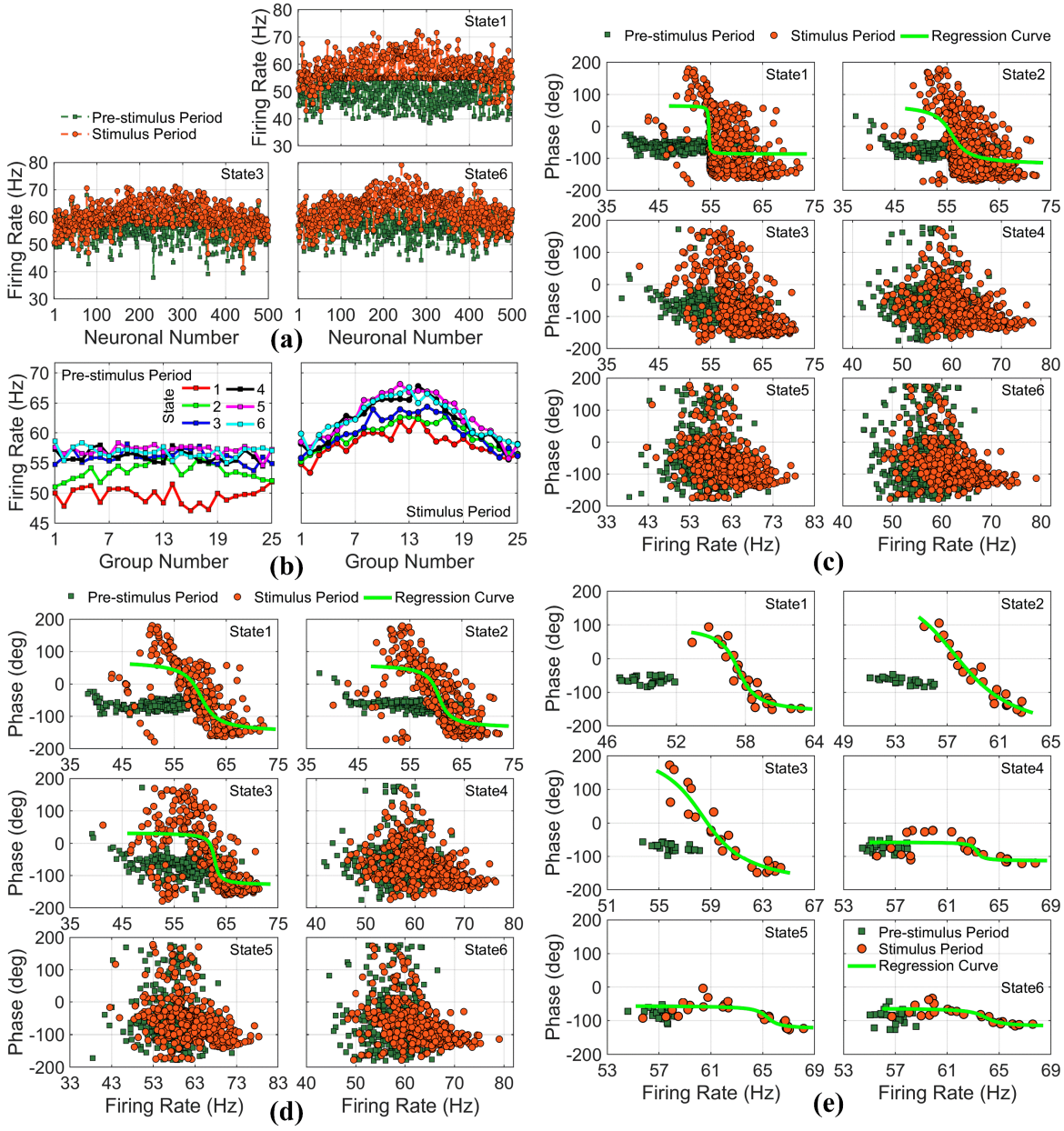

FIGURE 6. Relationship between Oscillatory Phase and Neuronal Excitation. (a) Neuronal firing rates for 500 individual neurons in state1, state3 and state6 during pre-stimulus and stimulus periods. (b) Neuronal firing rates for 25 neuronal groups in six network activity states during prestimulus and stimulus periods. (c) Relationships between spike-LFP phase and neuronal firing rate for all 500 individual neurons in six network activity states. (d) Similar to (c), but for individual neurons with lower PPC2 values (Not all the 500 individual neurons). (e) Relationships between spike-LFP phase and neuronal firing rate for 25 neuronal groups in six network activity states.

a goodness-of-fit statistic measure, acquired considerably lower values {0.323, 0.293}, which indicated large differences between the observed data and the fitted regression curves. From state3 to state 6, the spike-LFP phases were increasingly scattered and no obvious relationships could be evaluated.

Then we measured the relationships by selecting individual neurons with lower PPC2 values, under the thresholds {0.19, 0.18, 0.12, 0.03, 0.01, 0.005} for six network activity states respectively. Because neurons with lower PPC2 values were supposed to have more varying spike-LFP phases, shifting more randomly as opposed to being constrained to certain intervals in oscillatory cycles, therefore more appropriate for quantifying the relationships. Accordingly, we could quantify the relationships for more network activity states and finally established three regression curves for states from state1 to state3 (Fig. 6(d)). The R squared values were {0.575, 0.562, 0.468} (Table 2), which was to a certain extent better

TABLE 2. Parameter estimate for relationships between spike-LFP phase and neuronal excitation.

		State1	State2	State3	State4	State5	State6
FR-IDV	β	-8.212	-0.427	\	\	\	\
	R squared	0.323	0.293	\	\	\	\
FR-IDV-L	β	-0.432	-0.627	-1.449	\	\	\
	R squared	0.575	0.562	0.468	\	\	\
FR-GP	β	-0.860	-0.284	-0.391	-3.144	-1.485	-1.087
	R squared	0.909	0.946	0.910	0.482	0.656	0.700

FR-IDV: Firing Rate for Individual Neurons, FR-IDV-L: Firing Rate for Individual Neurons with Lower PPC2 Values, FR-GP: Firing Rate for Neuronal Groups

TABLE 3. Parameter estimate for relationships between spike-LFP phase and input strength.

		State1	State2	State3	State4	State5	State6
SCP	β	-0.205	-0.196	-0.205	\	\	\
	R squared	0.786	0.733	0.649	\	\	\
LFPP	β	-0.213	-0.197	-0.217	-0.599	-0.502	-0.503
	R squared	0.934	0.931	0.929	0.414	0.616	0.620
PR	β	-0.056	-0.057	-0.087	-0.088	-0.092	-0.031
	R squared	0.956	0.960	0.942	0.428	0.632	0.646

SCP: Synaptic Current Power, LFPP: LFP Power, PR: Poisson Rate

than the case of all 500 individual neurons illustrated above (Fig. 6(c)). Besides, the regression coefficients β $\{-0.432, -0.627, -1.449\}$ for the three curves were all negative as well. From state4 to state6, there is no apparent relationships available on account of more and more distributed spike-LFP phases.

As distinct from individual neurons with regression estimation available for only two or three network activity states, we could implement regression analysis of neuronal groups for all six network activity states (Fig. 6(e)). Based on Table 2, the R squared values were {0.909, 0.946, 0.910, 0.482, 0.656, 0.700}, significantly larger than the ones for individual neurons, indicating excellent model fittings and reliable relationship quantifications. Similar to individual neurons, we obtained the regression coefficient β with all negative values ($\{-0.860, -0.284, -0.391, -3.144, -1.485, -1.087\}$). Consequently, no matter individual neurons or neuronal groups, the oscillatory phase decreased monotonically as a function of neuronal firing rate and neuronal excitation, in good accordance with several evidences, including a theta-phase precession phenomenon [22], a gamma cycle hypothesis [19], a gamma-phase shifting experiment [21], and other numerical simulations [25], [33], [34]. More importantly, it is reasonable to conclude that neuronal groups have a competitive advantage over individual neurons to quantify the relationship between oscillatory phase and neuronal excitation.

E. RELATIONSHIP BETWEEN OSCILLATORY PHASE AND INPUT STRENGTH

In this section, we mainly explored the relationship between spike-LFP phase and input strength, characterized by synaptic current power for individual neurons, as well as LFP power and Poisson rate for neuronal groups. During pre-stimulus period in each network activity state, the synaptic current power and the LFP power were considerably flat and similar across orientation columns as a consequence of identical Poisson rate F_{bg} of external input and the same background current I_{bg} (Fig. 7(a, b)). During stimulus period in each network activity state, both the synaptic current power and the LFP power from middle orientation columns gained larger values, which declined progressively towards two-side columns. From state1 to state6, the synaptic current power and the LFP power became increasingly smaller. Once again, tuning curves of the synaptic current power and the LFP power not only confirmed orientation selectivity in visual cortex [56], [60], but also coincided with the distribution of Poisson rate for 25 Poisson groups determined previously (Fig. 1(d)).

Similarly, the synaptic current power, the LFP power and the Poisson rate were all linear predictor variables, however the spike-LFP phase was a circular variable. In consequence, we adopted a linear-circular regression model to measure the relationship as well, by way of Equation (20). Unlike the parameter configuration in the previous section, we customized the term $\alpha = 2$ at first. The parameter Y_i depicted a synaptic current power for the i^{th} individual neuron, an LFP power or a Poisson rate for the i^{th} neuronal group.

With respect to individual neurons, we simply formulated the relationship between the spike-LFP phase and the synaptic current power for all 500 individual neurons (Fig. 7(c)). Three regression curves with sliding slopes were determined for states from state1 to state3, the regression coefficients of which were all negative referring to Table 3 (β $\{-0.205, -0.196, -0.205\}$). Their corresponding statistics of R squared {0.786, 0.733, 0.649} were moderate, meaning that a more or less medium fitting of scattered data with the regression curves. From state4 to state6, the analytical relationships were no longer available as a consequence of increasingly dispersed spike-LFP phases.

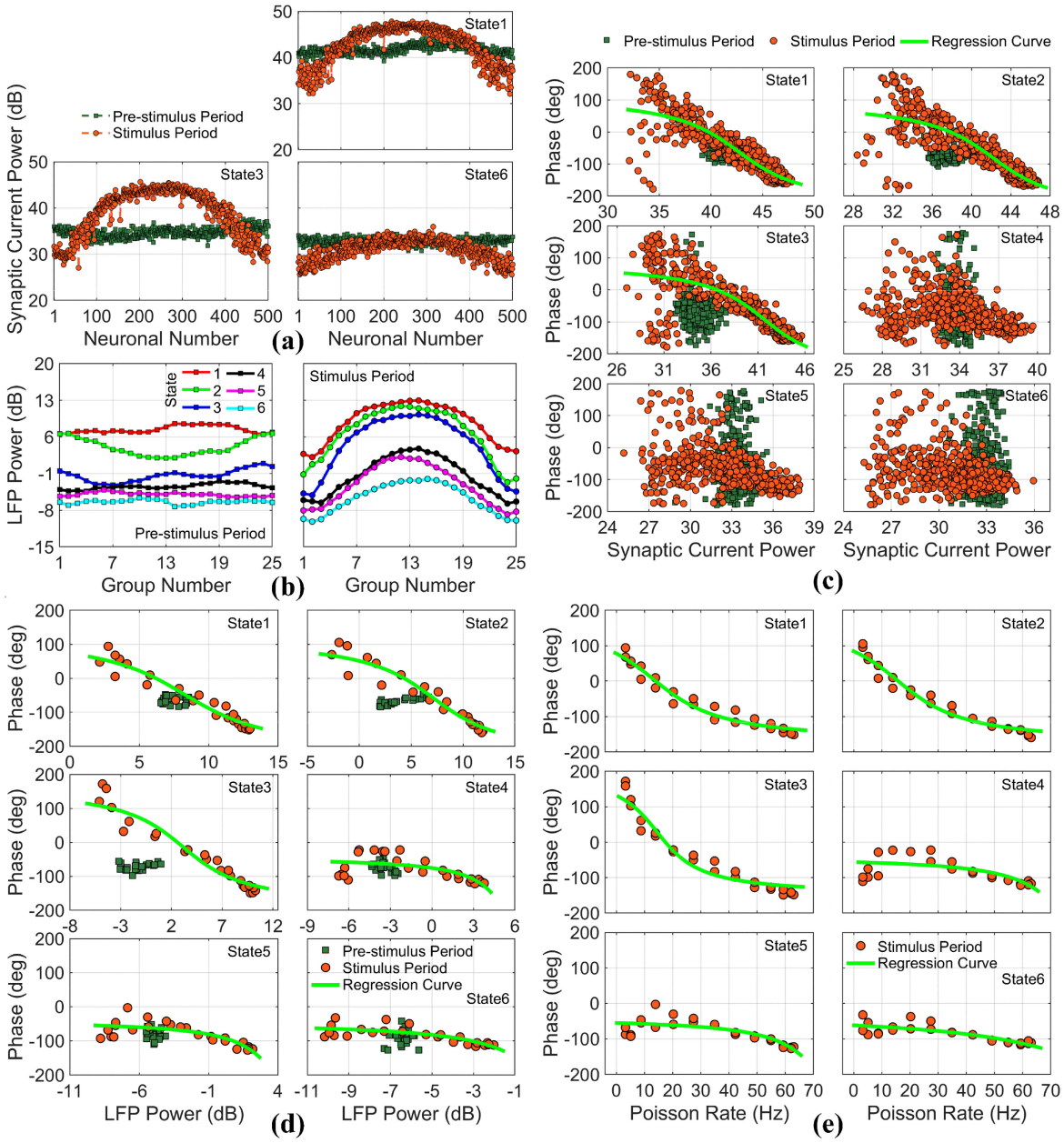

FIGURE 7. Relationship between Oscillatory Phase and Input Strength. (a) Synaptic current power for 500 individual neurons in state1, state3 and state6 during pre-stimulus and stimulus periods. (b) LFP power for 25 neuronal groups in six network activity states during pre-stimulus and stimulus periods. (c) Relationships between spike-LFP phase and synaptic current power for 500 individual neurons in six network activity states. (d) Relationships between spike-LFP phase and LFP power for 25 neuronal groups in six network activity states. (e) Relationships between spike-LFP phase and Poisson rate for 25 neuronal groups in six network activity states.

As far as neuronal groups were concerned, we could characterize the relationships of the spike-LFP phase with the LFP power and the Poisson rate for all six network activity states (Fig. 7(d, e)). Far more important was the outcome of considerably large values of R squared, {0.934, 0.931, 0.929, 0.414, 0.616, 0.620} for LFP power case and {0.956, 0.960, 0.942, 0.428, 0.632, 0.646} for Poisson rate case. It was infinitely superior to the case of individual neurons. Besides, on the basis of Table 3, the regression coefficients β for both LFP power and Poisson rate were all negative, consistent with the ones for the synaptic current power of individual neurons. It explicitly meant that the oscillatory phase decreased monotonically with input strength, in good agreement with a number of physiological experiments [19], [21], [22] and computational investigations [25], [33], [34]. In view of the relationship quantifications above, neuronal groups are supposed to be more suitable than individual neurons to measure the relationship between oscillatory phase and input strength.

F. TIME-RESOLVED ANALYSIS

In this section, we carried out a time-resolved analysis of spike-LFP phases for both individual neurons and neuronal groups with a sliding window, depicted by red rectangles

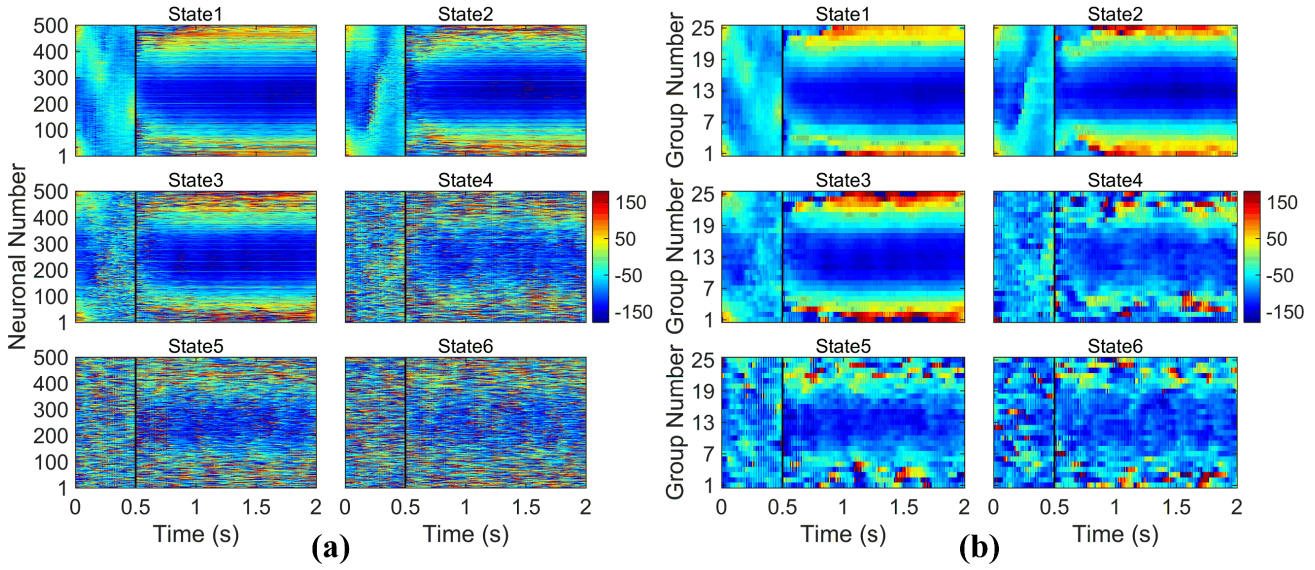

FIGURE 8. Time-resolved Analysis of Spike-LFP Phase. (a) Evolution of spike-LFP phases for 500 individual neurons across trial time in six network activity states. For each network state, the trial time consists of a 0.5 s pre-stimulus period and a 1.5 s stimulus period. (b) Similar to (a), but for the evolution of spike-LFP phases for 25 neuronal groups.

in Fig. 2(a). The width of the sliding window was 75 ms and the moving step was 10 ms. The analysis was performed for the whole trial time, without discarding the beginning part of recorded data for pre-stimulus and stimulus periods.

From state1 to state3 during pre-stimulus period, spike-LFP phases were comparatively similar across individual neurons and neuronal groups (Fig. 8). Besides, the spike-LFP phases in two-side orientation columns attained relatively higher values at the beginning of pre-stimulus period. The reason was that the beginning interval was to a certain extent influenced by orientation stimulus and neuronal activities of previous stimulus period. From state4 to state6 during this period, the spike-LFP phases shifted more and more vigorously.

From state1 to state3 during stimulus period, several findings can be implied from Fig. 8. Firstly, the evolution of spike-LFP phases for neuronal groups was to a great extent similar to the one for individual neurons. However, there were a number of fluctuations in middle orientation columns for individual neurons, sometimes with large spike-LFP phases. Whereas the spike-LFP phases for neuronal groups in the middle columns were extremely stable, with few outliers. Because individual neurons fired irregularly and were more easily dominated by Poisson-like noise [48]. Secondly, the evolution of spike-LFP phases for both neuronal groups and individual neurons at most time points was consistent with the distribution of spike-LFP phase determined previously, with large values in two-side columns and small values in middle columns. Thirdly, the spike-LFP phases for both neuronal groups and individual neurons were roughly similar across orientation columns at the beginning of stimulus period as a consequence of stimulus onset transient effect [3], [21]. Fourthly, in spite of receiving a constant orientation of input stimulus, there still existed variations in spike-LFP phase across trial time. From state4 to state6, the spike-LFP phases were more and more similar across individual neurons. However, there were still discrepancies between middle columns and two-side columns for neuronal groups, slightly better than the case of individual neurons.

IV. CONCLUSION AND DISCUSSION

In this paper, we primarily investigated oscillatory phase and phase synchronization, as well as relationships of the oscillatory phase with neuronal excitation and input strength for neuronal groups. For comparison, we investigated the same issues for individual neurons and then drew a parallel between the two cases to check if the group case was better than the individual case. Based on an electrophysiological study [21], we constructed 25 columns by a spiking neural network to simulate orientation columns in visual cortex, with 25 Poisson groups mimicking LGN and supplying thalamocortical inputs. All neurons throughout this paper were described by a leaky integrate-and-fire model and assigned with a preferred orientation according to the column number. For independent and comparative analyses, we introduced a pre-stimulus period and a stimulus period, as well as six network activity states regulated by Gaussian white noise. Other categories of neuronal models and noises can be adopted in this study, which does not qualitatively affect the results of the simulation. Besides, we also implemented a time-resolved analysis with a sliding window to measure the variation of oscillatory phase across trial time.

To quantify oscillatory phase for neuronal groups and individual neurons, we proposed a new method of spike-LFP phase based on vector addition of point spike-LFP phases across neurons and trials, instead of on the basis of averaging the point spike-LFP phases directly. To measure phase synchronization, we proposed a PPCG approach for neuronal

groups and adopted a PPC2 method for individual neurons. The neuronal excitation was represented by neuronal firing rate for both neuronal groups and individual neurons. Whereas the input strength was described by synaptic current power for individual neurons, along with LFP power and Poisson rate for neuronal groups.

There were several outcomes derived from the investigation. Firstly, gamma band oscillations existed in the neuronal network, supported by the frequencies of spike raster, LFP and synaptic current oscillations, the peak frequencies of LFP power and synaptic current power, as well as the significant regions of PPC2 and PPCG. It was in line with a wide range of physiological experiments [3], [5], [15] and computational models [26], [50]. Secondly, the properties of oscillatory phase and phase synchronization for neuronal groups were compatible with the ones for individual neurons. Thirdly, the vector addition phase was more suitable than the mean phase for representing oscillatory phase because of its closer to median phase. Fourthly, preferred orientation and stronger external input would give rise to smaller and more concentrated oscillatory phases. Besides, the oscillatory phase decreased monotonically as a function of neuronal excitation and input strength for both individual neurons and neuronal groups. It was in good agreement with a gamma cycle hypothesis [19], a theta-phase precession experiment [22], a gamma-phase shifting study [21] and other computational investigations [25], [33], [34]. Lastly, neuronal groups had a competitive advantage over individual neurons to measure the relationships of oscillatory phase with neuronal excitation and input strength. Because neuronal groups can establish reliable relationship quantifications for all six network activity states, whereas individual neurons can only measure the relationships for robust oscillatory states.

We have already explored this issue in a previous paper [34], which however is primarily for individual neurons. The major differences between the two studies are as follows. Firstly, in this paper, we proposed a PPCG method of phase synchronization for neuronal groups, which was simply measured by a mean PPC2 value averaged across individual neurons within a neuronal group in the previous paper. Secondly, we proposed a new spike-LFP phase method on the basis of vector addition of point spike-LFP phases in this simulation, and further elaborated the superiority of the vector addition phase. Thirdly, the relationship quantifications of oscillatory phase in the previous study were mainly for individual neurons, and with medium or even poor fitting effects. Whereas the relationship quantifications of oscillatory phase in the current study were for both individual neurons and neuronal groups, with neuronal groups having a considerable advantage over individual neurons. Furthermore, we also demonstrated phase synchronization and a time-resolved analysis for neuronal groups in this simulation.

Although our study was consistent with several physiological and computational investigations about the relationship between oscillatory phase and external input [21], [25], [33], there still exist a few discrepancies. Firstly, these investigations are primarily for individual neurons, whereas the ones in this paper are for both individual neurons and neuronal groups. A gamma-phase shifting study was carried out for individual neurons, which were isolated from MUA (Multiunit Activity) signals [21]. A phase-shifting computational study was implemented for periodically driven individual neurons at first and then for hyper-columns [25]. An information-transmission computational study was completely for individual neurons [33]. Secondly, the representations of oscillatory phase in these investigations are heterogeneous. The gamma-phase shifting study utilized a point spike-LFP phase relative to the spike time point, obtained through spectrum computation and within frequency domain [21]. The phase in the phase-shifting study was a relative phase, defined relative to an underlying oscillation, within time domain [25]. The phase in the information-transmission study was determined relative to the input sinusoidal signals directly, again within time domain [33]. However, in our simulation, the spike-LFP phase was computed approximately according to a physiological experiment procedure [21] and within frequency domain.

For future investigation, the PPCG method is supposed to be further explored to guarantee if it is biased by different number of spikes, neurons and trials. Besides, we would explore the relationship of phase synchronization with neuronal excitation and input strength for neuronal groups, and check if the group case is superior to the individual case. Furthermore, in view of the reliable findings of spike-LFP phase and PPCG for neuronal groups, we would investigate and further propose a feasible computational model for a cognitive function of object-based attention [17], [82], with object information coded by the spike-LFP phase of neuronal groups and selective attention flexibly coordinated by the PPCG method.

REFERENCES

[1] Y. B. Saalmann, M. A. Pinsk, L. Wang, X. Li, and S. Kastner, "The pulvinar regulates information transmission between cortical areas based on attention demands," *Science*, vol. 337, no. 6095, pp. 753–756, Aug. 2012.

[2] G. G. Gregoriou, S. J. Gotts, H. Zhou, and R. Desimone, "High-frequency, long-range coupling between prefrontal and visual cortex during attention," *Science*, vol. 324, no. 5931, pp. 1207–1210, May 2009.

[3] P. Fries, "Modulation of oscillatory neuronal synchronization by selective visual attention," *Science*, vol. 291, no. 5508, pp. 1560–1563, Feb. 2001.

[4] J.-M. Schoffelen, "Neuronal coherence as a mechanism of effective corticospinal interaction," *Science*, vol. 308, no. 5718, pp. 111–113, Apr. 2005.

[5] M. Carus-Cadavieco, M. Gorbati, L. Ye, F. Bender, S. van der Veldt, C. Kosse, C. Börgers, S. Y. Lee, C. Ramakrishnan, Y. Hu, N. Denisova, F. Ramm, E. Volitaki, D. Burdakov, K. Deisseroth, A. Ponomarenko, and T. Korotkova, "Gamma oscillations organize top-down signalling to hypothalamus and enable food seeking," *Nature*, vol. 542, no. 7640, pp. 232–236, Feb. 2017.

[6] C. Dejean, J. Courtin, N. Karalis, F. Chaudun, H. Wurtz, T. C. M. Bienvenu, and C. Herry, "Prefrontal neuronal assemblies temporally control fear behaviour," *Nature*, vol. 535, no. 7612, pp. 420–424, Jul. 2016.

[7] T. Spellman, M. Rigotti, S. E. Ahmari, S. Fusi, J. A. Gogos, and J. A. Gordon, "Hippocampal-prefrontal input supports spatial encoding in working memory," *Nature*, vol. 522, no. 7556, pp. 309–314, Jun. 2015.

[8] K. M. Igarashi, L. Lu, L. L. Colgin, M. Moser, and E. I. Moser, "Coordination of entorhinal-hippocampal ensemble activity during associative learning," *Nature*, vol. 510, no. 7503, pp. 143–147, Jun. 2014.

[9] K. D. Harris, J. Csicsvari, H. Hirase, G. Dragoi, and G. Buzsáki, "Organization of cell assemblies in the hippocampus," *Nature*, vol. 424, no. 6948, pp. 552–556, Jul. 2003.
[10] J. A. Cardin, M. Carlén, K. Meletis, U. Knoblich, F. Zhang, K. Deisseroth, L.-H. Tsai, and C. I. Moore, "Driving fast-spiking cells induces gamma rhythm and controls sensory responses," *Nature*, vol. 459, no. 7247, pp. 663–667, Apr. 2009.
[11] M. Smear, R. Shusterman, R. O'Connor, T. Bozza, and D. Rinberg, "Perception of sniff phase in mouse olfaction," *Nature*, vol. 479, no. 7373, pp. 397–400, Oct. 2011.
[12] J. Courtin, F. Chaudun, R. R. Rozeske, N. Karalis, C. Gonzalez-Campo, H. Wurtz, A. Abdi, J. Baufreton, T. C. M. Bienvenu, and C. Herry, "Prefrontal parvalbumin interneurons shape neuronal activity to drive fear expression," *Nature*, vol. 505, no. 7481, pp. 92–96, Jan. 2014.
[13] G. Laurent and H. Davidowitz, "Encoding of olfactory information with oscillating neural assemblies," *Science*, vol. 265, no. 5180, pp. 1872–1875, Sep. 1994.
[14] E. Pastalkova, V. Itskov, A. Amarasingham, and G. Buzsaki, "Internally generated cell assembly sequences in the rat hippocampus," *Science*, vol. 321, no. 5894, pp. 1322–1327, Sep. 2008.
[15] T. Womelsdorf, J.-M. Schoffelen, R. Oostenveld, W. Singer, R. Desimone, A. K. Engel, and P. Fries, "Modulation of neuronal interactions through neuronal synchronization," *Science*, vol. 316, no. 5831, pp. 1609–1612, Jun. 2007.
[16] R. F. Salazar, N. M. Dotson, S. L. Bressler, and C. M. Gray, "Content-specific fronto-parietal synchronization during visual working memory," *Science*, vol. 338, no. 6110, pp. 1097–1100, Nov. 2012.
[17] D. Baldauf and R. Desimone, "Neural mechanisms of object-based attention," *Science*, vol. 344, no. 6182, pp. 424–427, Apr. 2014.
[18] L. L. Colgin, T. Denninger, M. Fyhn, T. Hafting, T. Bonnevie, O. Jensen, M.-B. Moser, and E. I. Moser, "Frequency of gamma oscillations routes flow of information in the hippocampus," *Nature*, vol. 462, no. 7271, pp. 353–357, Nov. 2009.
[19] P. Fries, D. Nikolic, and W. Singer, "The gamma cycle," *Trends Neurosci.*, vol. 30, no. 7, pp. 309–316, Jul. 2007.
[20] M. A. Montemurro, M. J. Rasch, Y. Murayama, N. K. Logothetis, and S. Panzeri, "Phase-of-firing visual stimuli in coding of natural primary visual cortex," *Current Biol.*, vol. 18, no. 5, pp. 375–380, Mar. 2008.
[21] M. Vinck, B. Lima, T. Womelsdorf, R. Oostenveld, W. Singer, S. Neuenschwander, and P. Fries, "Gamma-phase shifting in awake monkey visual cortex," *J. Neurosci.*, vol. 30, no. 4, pp. 1250–1257, Jan. 2010.
[22] J. O'Keefe and M. L. Recce, "Phase relationship between hippocampal place units and the EEG theta rhythm," *Hippocampus*, vol. 3, no. 3, pp. 317–330, Jul. 1993.
[23] C. Kayser, M. A. Montemurro, N. K. Logothetis, and S. Panzeri, "Spike-phase coding boosts and stabilizes information carried by spatial and temporal spike patterns," *Neuron*, vol. 61, no. 4, pp. 597–608, Feb. 2009.
[24] M. Siegel, M. R. Warden, and E. K. Miller, "Phase-dependent neuronal coding of objects in short-term memory," *Proc. Nat. Acad. Sci. USA*, vol. 106, no. 50, pp. 21341–21346, Nov. 2009.
[25] P. H. Tiesinga and T. J. Sejnowski, "Mechanisms for phase shifting in cortical networks and their role in communication through coherence," *Frontiers Hum. Neurosci.*, vol. 4, p. 196, Nov. 2010.
[26] E. Lowet, M. Roberts, A. Hadjipapas, A. Peter, J. van der Eerden, and P. De Weerd, "Input-dependent frequency modulation of cortical gamma oscillations shapes spatial synchronization and enables phase coding," *PLOS Comput. Biol.*, vol. 11, no. 2, Feb. 2015, Art. no. e1004072.
[27] S. Quax, O. Jensen, and P. Tiesinga, "Top-down control of cortical gamma-band communication via pulvinar induced phase shifts in the alpha rhythm," *PLOS Comput. Biol.*, vol. 13, no. 5, May 2017, Art. no. e1005519.
[28] M. T. Wal and P. H. Tiesinga, "Phase difference between model cortical areas determines level of information transfer," *Frontiers Comput. Neurosci.*, vol. 11, p. 6, Feb. 2017.
[29] R. F. Helfrich, T. R. Schneider, S. Rach, S. A. Trautmann-Lengsfeld, A. K. Engel, and C. S. Herrmann, "Entrainment of brain oscillations by transcranial alternating current stimulation," *Current Biol.*, vol. 24, no. 3, pp. 333–339, Feb. 2014.
[30] R. Polanía, M. A. Nitsche, C. Korman, G. Batsikadze, and W. Paulus, "The importance of timing in segregated theta phase-coupling for cognitive performance," *Current Biol.*, vol. 22, no. 14, pp. 1314–1318, Jul. 2012.
[31] M. Vinck, M. van Wingerden, T. Womelsdorf, P. Fries, and C. M. A. Pennartz, "The pairwise phase consistency: A bias-free measure of rhythmic neuronal synchronization," *NeuroImage*, vol. 51, no. 1, pp. 112–122, May 2010.
[32] M. Vinck, F. P. Battaglia, T. Womelsdorf, and C. Pennartz, "Improved measures of phase-coupling between spikes and the local field potential," *J. Comput. Neurosci.*, vol. 33, no. 1, pp. 53–75, Aug. 2012.
[33] S. Gielen, M. Krupa, and M. Zeitler, "Gamma oscillations as a mechanism for selective information transmission," *Biol. Cybern.*, vol. 103, no. 2, pp. 151–165, Apr. 2010.
[34] D. Wang, Y. Sun, F. Wang, and J. Li, "Modeling oscillatory phase and phase synchronization with neuronal excitation and input strength in cortical network," *IEEE Access*, vol. 6, pp. 36441–36458, 2018.
[35] D. H. Hubel and T. N. Wiesel, "Receptive fields of single neurones in the cat's striate cortex," *J. Physiol.*, vol. 148, no. 3, pp. 574–591, Oct. 1959.
[36] J. Fritz, S. Shamma, M. Elhilali, and D. Klein, "Rapid task-related plasticity of spectrotemporal receptive fields in primary auditory cortex," *Nature Neurosci.*, vol. 6, no. 11, pp. 1216–1223, Oct. 2003.
[37] R. Q. Quiroga, L. Reddy, G. Kreiman, C. Koch, and I. Fried, "Invariant visual representation by single neurons in the human brain," *Nature*, vol. 435, no. 7045, pp. 1102–1107, Jun. 2005.
[38] M. Ainsworth, S. Lee, M. O. Cunningham, R. D. Traub, N. J. Kopell, and M. A. Whittington, "Rates and rhythms: A synergistic view of frequency and temporal coding in neuronal networks," *Neuron*, vol. 75, no. 4, pp. 572–583, Aug. 2012.
[39] A. Z. Harris and J. A. Gordon, "Long-range neural synchrony in behavior," *Annu. Rev. Neurosci.*, vol. 38, no. 1, pp. 171–194, Jul. 2015.
[40] J. Wagemans, J. H. Elder, M. Kubovy, S. E. Palmer, M. A. Peterson, M. Singh, and R. von der Heydt, "A century of gestalt psychology in visual perception: I. perceptual grouping and figure-ground organization.," *Psychol. Bull.*, vol. 138, no. 6, pp. 1172–1217, Nov. 2012.
[41] F. Duret, S. Shumikhina, and S. Molotchnikoff, "Neuron participation in a synchrony-encoding assembly," *BMC Neurosci.*, vol. 7, no. 1, p. 72, Oct. 2006.
[42] A. Engel, P. Konig, A. Kreiter, and W. Singer, "Interhemispheric synchronization of oscillatory neuronal responses in cat visual cortex," *Science*, vol. 252, no. 5009, pp. 1177–1179, May 1991.
[43] W. Singer and C. M. Gray, "Visual feature integration and the temporal correlation hypothesis," *Annu. Rev. Neurosci.*, vol. 18, no. 1, pp. 555–586, Mar. 1995.
[44] C. A. Bosman, C. S. Lansink, and C. M. A. Pennartz, "Functions of gamma-band synchronization in cognition: From single circuits to functional diversity across cortical and subcortical systems," *Eur. J. Neurosci.*, vol. 39, no. 11, pp. 1982–1999, May 2014.
[45] J. M. Samonds, J. D. Allison, H. A. Brown, and A. B. Bonds, "Cooperative synchronized assemblies enhance orientation discrimination," *Proc. Nat. Acad. Sci. USA*, vol. 101, no. 17, pp. 6722–6727, Apr. 2004.
[46] G. Dragoi and G. Buzsáki, "Temporal encoding of place sequences by hippocampal cell assemblies," *Neuron*, vol. 50, no. 1, pp. 145–157, Apr. 2006.
[47] M. Zeitler, P. Fries, and S. Gielen, "Assessing neuronal coherence with single-unit, multi-unit, and local field potentials," *Neural Comput.*, vol. 18, no. 9, pp. 2256–2281, Sep. 2006.
[48] T. Akam and D. M. Kullmann, "Oscillations and filtering networks support flexible routing of information," *Neuron*, vol. 67, no. 2, pp. 308–320, Jul. 2010.
[49] R. Brette, "Computing with neural synchrony," *PLoS Comput. Biol.*, vol. 8, no. 6, Jun. 2012, Art. no. e1002561.
[50] A. Barardi, B. Sancristóbal, and J. Garcia-Ojalvo, "Phase-coherence transitions and communication in the gamma range between delay-coupled neuronal populations," *PLoS Comput. Biol.*, vol. 10, no. 7, Jul. 2014, Art. no. e1003723.
[51] R. J. Douglas and K. A. C. Martin, "Neuronal circuits of the neocortex," *Annu. Rev. Neurosci.*, vol. 27, no. 1, pp. 419–451, Jul. 2004.
[52] C. A. Bosman, J.-M. Schoffelen, N. Brunet, R. Oostenveld, A. M. Bastos, T. Womelsdorf, B. Rubehn, T. Stieglitz, P. De Weerd, and P. Fries, "Attentional stimulus selection through selective synchronization between monkey visual areas," *Neuron*, vol. 75, no. 5, pp. 875–888, Sep. 2012.
[53] A. M. Bastos, W. M. Usrey, R. A. Adams, G. R. Mangun, P. Fries, and K. J. Friston, "Canonical microcircuits for predictive coding," *Neuron*, vol. 76, no. 4, pp. 695–711, Nov. 2012.
[54] H. Hu, J. Gan, and P. Jonas, "Fast-spiking, parvalbumin(+) GABAergic interneurons: From cellular design to microcircuit function," *Science*, vol. 345, no. 6196, Jul. 2014, 1255263.

[55] M. Zeitler, P. Fries, and S. Gielen, "Biased competition through variations in amplitude of γ-oscillations," *J. Comput. Neurosci.*, vol. 25, no. 1, pp. 89–107, Feb. 2008.
[56] D. Ferster and K. D. Miller, "Neural mechanisms of orientation selectivity in the visual cortex," *Annu. Rev. Neurosci.*, vol. 23, no. 1, pp. 441–471, Mar. 2000.
[57] D. H. Hubel and T. N. Wiesel, "Receptive fields and functional architecture of monkey striate cortex," *J. Physiol.*, vol. 195, no. 1, pp. 215–243, Mar. 1968.
[58] T. P. Vogels, H. Sprekeler, F. Zenke, C. Clopath, and W. Gerstner, "Inhibitory plasticity balances excitation and inhibition in sensory pathways and memory networks," *Science*, vol. 334, no. 6062, pp. 1569–1573, Nov. 2011.
[59] R. C. Reid, "From functional architecture to functional connectomics," *Neuron*, vol. 75, no. 2, pp. 209–217, Jul. 2012.
[60] D. H. Hubel and T. N. Wiesel, "Receptive fields, binocular interaction and functional architecture in the cat's visual cortex," *J. Physiol.*, vol. 160, no. 1, pp. 106–154, Jan. 1962.
[61] H. Markram, M. Toledo-Rodriguez, Y. Wang, A. Gupta, G. Silberberg, and C. Wu, "Interneurons of the neocortical inhibitory system," *Nature Rev. Neurosci.*, vol. 5, no. 10, pp. 793–807, Oct. 2004.
[62] B. Sancristóbal, R. Vicente, and J. Garcia-Ojalvo, "Role of frequency mismatch in neuronal communication through coherence," *J. Comput. Neurosci.*, vol. 37, no. 2, pp. 193–208, Feb. 2014.
[63] D. Somers, S. Nelson, and M. Sur, "An emergent model of orientation selectivity in cat visual cortical simple cells," *J. Neurosci.*, vol. 15, no. 8, pp. 5448–5465, Aug. 1995.
[64] M. Kaiser, C. C. Hilgetag, and A. van Ooyen, "A simple rule for axon outgrowth and synaptic competition generates realistic connection lengths and filling fractions," *Cerebral Cortex*, vol. 19, no. 12, pp. 3001–3010, May 2009.
[65] N. Brunel and D. Hansel, "How noise affects the synchronization properties of recurrent networks of inhibitory neurons," *Neural Comput.*, vol. 18, no. 5, pp. 1066–1110, May 2006.
[66] S. Ostojic, N. Brunel, and V. Hakim, "Synchronization properties of networks of electrically coupled neurons in the presence of noise and heterogeneities," *J. Comput. Neurosci.*, vol. 26, no. 3, pp. 369–392, Jun. 2009.
[67] X. Jia, D. Xing, and A. Kohn, "No consistent relationship between gamma power and peak frequency in macaque primary visual cortex," *J. Neurosci.*, vol. 33, no. 1, pp. 17–25, Jan. 2013.
[68] A. Buehlmann and G. Deco, "Optimal information transfer in the cortex through synchronization," *PLoS Comput. Biol.*, vol. 6, no. 9, Sep. 2010, Art. no. e1000934.
[69] D. F. M. Goodman, "The brian simulator," *Frontiers Neurosci.*, vol. 3, no. 2, pp. 192–197, Sep. 2009.
[70] R. Oostenveld, P. Fries, E. Maris, and J.-M. Schoffelen, "FieldTrip: Open source software for advanced analysis of MEG, EEG, and invasive electrophysiological data," *Comput. Intell. Neurosci.*, vol. 2011, Dec. 2011, Art. no. 156869.
[71] A. Mazzoni, S. Panzeri, N. K. Logothetis, and N. Brunel, "Encoding of naturalistic stimuli by local field potential spectra in networks of excitatory and inhibitory neurons," *PLoS Comput. Biol.*, vol. 4, no. 12, Dec. 2008, Art. no. e1000239.
[72] P. Fries, "Neuronal gamma-band synchronization as a fundamental process in cortical computation," *Annu. Rev. Neurosci.*, vol. 32, no. 1, pp. 209–224, Jun. 2009.
[73] M. J. Roberts, E. Lowet, N. M. Brunet, M. Ter Wal, P. Tiesinga, P. Fries, and P. De Weerd, "Robust gamma coherence between macaque V1 and V2 by dynamic frequency matching," *Neuron*, vol. 78, no. 3, pp. 523–536, May 2013.
[74] J. Cannon, M. M. McCarthy, S. Lee, J. Lee, C. Börgers, M. A. Whittington, and N. Kopell, "Neurosystems: Brain rhythms and cognitive processing," *Eur. J. Neurosci.*, vol. 39, no. 5, pp. 705–719, Mar. 2014.
[75] S. Ray and J. H. R. Maunsell, "Differences in gamma frequencies across visual cortex restrict their possible use in computation," *Neuron*, vol. 67, no. 5, pp. 885–896, Sep. 2010.
[76] P. Fries, "A mechanism for cognitive dynamics: Neuronal communication through neuronal coherence," *Trends Cognit. Sci.*, vol. 9, no. 10, pp. 474–480, Oct. 2005.
[77] P. Fries, "Rhythms for cognition: Communication through coherence," *Neuron*, vol. 88, no. 1, pp. 220–235, Oct. 2015.
[78] R. Eckhorn, R. Bauer, W. Jordan, M. Brosch, W. Kruse, M. Munk, and H. J. Reitboeck, "Coherent oscillations: A mechanism of feature linking in the visual cortex? Multiple electrode and correlation analyses in the cat," *Biol. Cybern.*, vol. 60, no. 2, pp. 121–130, Dec. 1988.
[79] P. Fries, S. Neuenschwander, A. K. Engel, R. Goebel, and W. Singer, "Rapid feature selective neuronal synchronization through correlated latency shifting," *Nature Neurosci.*, vol. 4, no. 2, pp. 194–200, Feb. 2001.
[80] C. Börgers and N. J. Kopell, "Gamma oscillations and stimulus selection," *Neural Comput.*, vol. 20, no. 2, pp. 383–414, Feb. 2008.
[81] N. I. Fisher and A. J. Lee, "Regression models for an angular response," *Biometrics*, vol. 48, no. 3, p. 665, Sep. 1992.
[82] T. J. Buschman and S. Kastner, "From behavior to neural dynamics: An integrated theory of attention," *Neuron*, vol. 88, no. 1, pp. 127–144, Oct. 2015.

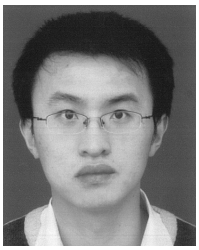

DAMING WANG graduated from the Department of Computer Science and Technology, Tongji University, Shanghai, China. His current research interests include computational neuroscience, brain rhythms, visual attention, and machine learning.

YAORU SUN received the Ph.D. degree in artificial intelligence from The University of Edinburgh. He is currently a Full Professor with the Department of Computer Science and Technology, Tongji University, China. His research interests include brian-like computation, machine intelligence, and cognitive neuroscience.

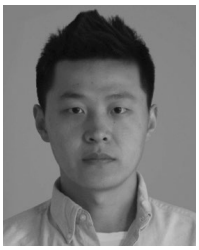

HAIBO SHI received the Ph.D. degree in pattern recognition and intelligent system from Tongji University, Shanghai, China. His research interests include deep reinforcement learning and cognitive computation.

FANG WANG is currently a Senior Lecturer with the Department of Computer Science, Brunel University, U.K. She has published many articles and filed a number of patents. Her research interests include software agents, cognitive neuroscience, and distributed computing. She received several technical awards.